

# Programmable $N$ -Body Interactions with Trapped Ions

Or Katz<sup>1,2,3,\*</sup>, Marko Cetina<sup>1,3</sup> and Christopher Monroe<sup>1,2,3,4</sup>

<sup>1</sup>*Duke Quantum Center, Duke University, Durham, North Carolina 27701, USA*

<sup>2</sup>*Department of Electrical and Computer Engineering, Duke University, Durham, North Carolina 27708, USA*

<sup>3</sup>*Department of Physics, Duke University, Durham, North Carolina 27708, USA*

<sup>4</sup>*IonQ, Inc., College Park, Maryland 20740, USA*



(Received 21 July 2022; accepted 8 June 2023; published 26 July 2023)

Trapped atomic ion qubits or effective spins are a powerful quantum platform for quantum computation and simulation, featuring densely connected and efficiently programmable interactions between the spins. While native interactions between trapped-ion spins are typically pairwise, many quantum algorithms and quantum spin models naturally feature couplings between triplets, quartets, or higher orders of spins. Here, we formulate and analyze a mechanism that extends the standard Mølmer-Sørensen pairwise entangling gate and generates a controllable and programmable coupling between  $N$  spins of trapped ions. We show that spin-dependent optical parametric drives applied at twice the motional frequency generate a coordinate transformation of the collective ion motion in phase space, rendering displacement forces that are nonlinear in the spin operators. We formulate a simple framework that enables a systematic and faithful construction of high-order spin Hamiltonians and gates, including the effect of multiple modes of motion, and characterize the performance of such operations under realistic conditions.

DOI: [10.1103/PRXQuantum.4.030311](https://doi.org/10.1103/PRXQuantum.4.030311)

## I. INTRODUCTION

Ions in a linear Paul trap are a salient platform for simulation of quantum spin dynamics [1] and for computation of problems that are classically hard [2]. Internal electronic energy levels of individual ions can be used as qubits or effective spins that can be efficiently prepared, controlled, and measured with high isolation from the environment. When trapped ions are laser cooled and ordered into long chains, their Coulomb interaction gives rise to collective modes of motion between the ions. With the addition of optical [3] or near-field microwave [4] driving fields, the resultant force can depend upon the quantum spin state of the ions, thus generating spin-spin entanglement and allowing for control over their many-body quantum state.

The most prominent configuration for such entangling operations uses bichromatic optical fields, which exert spin-dependent forces that displace the ions and result in the accumulation of a geometric spin-dependent phase [5–7]. This mechanism forms the basis for two-qubit Mølmer Sørensen (MS) gates widely used in trapped-ion

quantum computers, as well as effective Ising couplings in trapped-ion-based quantum simulators [1,8–14]. This engineered Ising coupling features dense or even full connectivity between pairs of ions, owing to their collective vibrations in a chain, but it is limited to two-body interactions.

Most quantum circuits and many spin models call for higher-order interactions. Examples including the simulation of molecular orbitals in quantum chemistry [15–19], quantum simulations of lattice gauge theories [20–23], stabilizer operators in quantum error-correction codes [24, 25], spin models [26–30] and generic quantum algorithms [31–37]. While sequential or parallel application of universal one- and two-body gate sets can generate arbitrary entangled many-body states, such constructions can carry overhead in the number of entangling operations or Trotterization steps [38] and thereby be limited in the face of decoherence.

Recently, we have proposed a mechanism to realize a native  $N$ -body interaction between trapped-ion spins by squeezing a single vibrational mode of motion in a state-dependent manner [39]. We have considered optical spin-dependent parametric drives that are applied synchronously at twice the motional frequency of a particular vibrational mode of motion, generating a family of  $N$ -body entangling interactions and gates that can be realized in a single step. In this paper, we extend that study by fully considering the coupling to multiple motional

\*Corresponding author: [or.katz@duke.edu](mailto:or.katz@duke.edu)

*Published by the American Physical Society under the terms of the [Creative Commons Attribution 4.0 International](https://creativecommons.org/licenses/by/4.0/) license. Further distribution of this work must maintain attribution to the author(s) and the published article's title, journal citation, and DOI.*

modes in the trapped-ion crystal. While the conventional MS-type interaction can be straightforwardly extended to off-resonant drives and multimode operation [40–46], the nonlinear nature of squeezing parametric drives renders the vibratory and spin evolution nontrivial owing to the quadratic dependence of the phonon operators in the interaction Hamiltonian. The treatment of multimode and off-resonant squeezing operations is also important in practice, as the parametric drives at twice the motional mode frequencies are generally accompanied by driving nearby off-resonant transitions that can play an important role in the dynamics [39].

Here, we analyze the application of time-dependent squeezing acting simultaneously on multiple motional modes of a trapped-ion chain. We formulate and characterize the evolution of the spin and motional states of the ions, revealing a large toolbox of effective spin Hamiltonians and quantum gates. We identify a particular protocol for combining multimode squeezing and displacement operations to demonstrate particular applications, including the construction of the  $N$ -body stabilizer operator composed of a product of  $N$  spin operators, as well as extensions of the  $N$ -bit Toffoli gate using multiple modes. Finally, we outline and demonstrate new avenues to program and simulate Hamiltonians composed of multiple high-order terms in a single step.

This paper is organized as follows. In Sec. II, we describe the time-dependent interaction Hamiltonian coupling the spins and motion of the ions. The resulting time evolution is composed of spin-dependent motional squeezing and displacements that are controlled by the optical fields. In Sec. III, we find that this evolution, in the Heisenberg picture, is described by a spin-dependent linear coordinate transformation in phase space. In Sec. IV, we use this linear transformation to construct a family of gates that act on the spins to generate  $N$ -body interactions that are robust to thermal motion of ions. In Sec. V, we present two numerical examples of gates that entangle four spins in a chain of 11 ions and show that nearby off-resonant motional modes can be controlled via pulse shaping. Finally, in Sec. VI we discuss the practical application of these gates to current trapped-ion systems and their prospects in other quantum hardware.

## II. INTERACTION HAMILTONIAN

We consider a linear chain of  $M$  trapped atomic ions, each storing a spin-1/2 system, addressed by laser beams, as shown in Fig. 1. We assume that  $M$  motional modes of the ions are aligned with the spatial direction of the effective optical axis. These modes are described by their frequencies  $\omega_k$  and displacement eigenvectors  $b_{ik}$ , which describe the motional amplitude of the  $i$ th ion in the  $k$ th motional mode normalized such that  $\sum_i b_{ik}b_{im} = \delta_{km}$  and  $\sum_k b_{ik}b_{jk} = \delta_{ij}$ . The phonon modes are characterized by

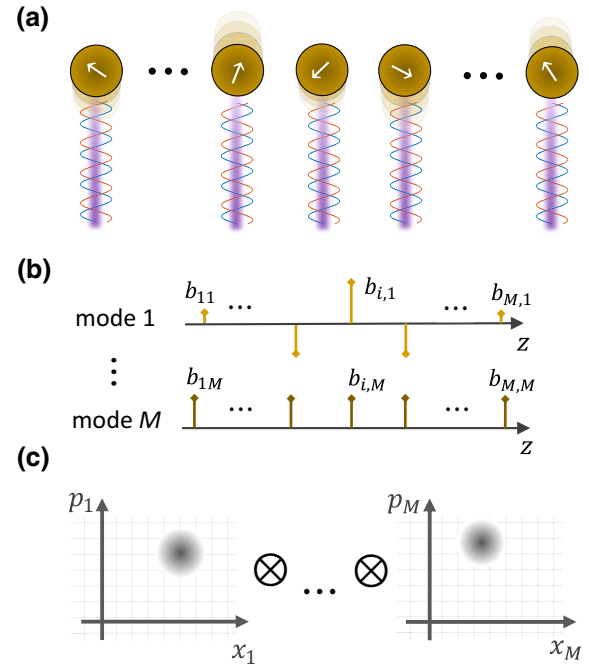


FIG. 1. The trapped-ion system. (a) A crystal of  $M$  ion spins trapped by external forces and addressed with an array of bichromatic optical fields. The beams apply state-dependent operations that couple the spin state of the ions with their motion. (b) Motion along the beam axis is composed of  $M$  collective vibrational modes of the crystal. The matrix element  $b_{ik}$  denotes the participation of the  $i$ th ion in the  $k$ th vibrational mode. (c) The vibrations of the crystal can be pictorially represented by  $M$  phase-space diagrams with coordinates  $\hat{x}_k$  and  $\hat{p}_k$  for  $1 \leq k \leq M$ . The coordinates are unitless (scaled to twice the zero-point position and momentum spreads) and described in the interaction frame, which rotates at the vibrational frequency  $\omega_k$  of the  $k$ th mode, such that the motional state in phase space is stationary unless optical fields are applied. The shaded area represents an arbitrary motional state of the crystal in each phonon mode.

the bosonic annihilation and creation operators  $\hat{a}_k$  and  $\hat{a}_k^\dagger$  of mode  $k$ , with  $[\hat{a}_k, \hat{a}_k^\dagger] = 1$ .

The applied optical fields couple the ion spins to their motion via the interaction Hamiltonian [47]

$$H_I = \frac{\hbar}{2} \sum_{i=1}^M \tilde{\Omega}_i(t) \sigma_+^{(i)} \prod_{k=1}^M e^{in_{ik}(\hat{a}_k e^{-i\omega_k t} + \hat{a}_k^\dagger e^{i\omega_k t})} + \text{h.c.}, \quad (1)$$

where the exponential term describes modulation of the optical phase in the reference frame of the oscillating ions. Here,  $\tilde{\Omega}_i(t)$  is the driving Rabi frequency for spin  $i$  in a frame rotating at the frequency of the  $i$ th spin and  $\sigma_\pm^{(i)}$  are the raising (+) and lowering (−) spin operators. The Lamb-Dicke parameters  $\eta_{ik} = \delta K x_k^0 b_{ik}$  describe the coupling between spin  $i$  and mode  $k$ , where  $\delta K$  is the effective wave number of the radiation field driving the sidebands and  $x_k^0 = \sqrt{\hbar/2M\omega_k}$  is the zero-point spread in position

of the  $k$ th phonon mode, taking  $\mathcal{M}$  as the mass of a single ion [47]. We assume that the radial motion along the optical beam is confined within the Lamb-Dicke regime, where  $|\eta_{ik}\langle\hat{a}_k^\dagger + \hat{a}_k\rangle| \ll 1$  for all ions and modes. While we assume that the above spin-motion coupling originates from either a direct optical transition or a twin-beam optical Raman process between spin states [47], the framework here can also be applied to a microwave drive with field gradients [4,48–50].

In phase space,  $H_I$  acts on the motional state of the ions as shown in Fig. 1(c). The phase-space coordinates of mode  $k$  are defined by the unitless quadrature position and momentum operators  $\hat{x}_k = (\hat{a}_k + \hat{a}_k^\dagger)/2$  and  $\hat{p}_k = i(\hat{a}_k^\dagger - \hat{a}_k)/2$ , which are scaled by  $2x_k^0$  and  $2p_k^0 = \sqrt{2\hbar\mathcal{M}\omega_k}$ , respectively. These operators satisfy  $[\hat{x}_k, \hat{p}_m] = i\delta_{km}/2$ .

In this work, we focus on the symmetric driving of the blue and red motional sidebands in Eq. (1). These bichromatic electromagnetic fields  $\tilde{\Omega}_i = \Omega_i(t)[e^{-i(\nu t + \phi_{i+})} + e^{i(\nu t - \phi_{i-})}]$  are applied with frequencies  $\pm\nu$  from the spin-resonance carrier, with phases  $\phi_{i\pm}$  and common amplitude  $\Omega_i(t)$ .

Tuning near the first motional sidebands with detunings  $\delta_k \equiv \nu - \omega_k$  from the frequencies of the motional modes, where  $|\delta_k| \ll \min(\{\omega_m | 1 \leq m \leq M\})$ , generates the interaction Hamiltonian under the rotating-wave approximation, where  $\Omega_i \ll \min(\{\omega_m | 1 \leq m \leq M\})$  [1]:

$$H_D = \frac{\hbar}{2} \sum_{k,i} \eta_{ik} \Omega_i(t) e^{i(\delta_k t + \delta\varphi_i)} \sigma_{\bar{\varphi}_i}^{(i)} \hat{a}_k + \text{h.c.} \quad (2)$$

Here,  $\delta\varphi_i = (\phi_{i+} - \phi_{i-})/2$  is the relative phase between the two tones and  $\bar{\varphi}_i = (\phi_{i+} + \phi_{i-} - \pi)/2$  is the common phase that determines the orientation of the spin operator on the Bloch sphere,  $\sigma_{\bar{\varphi}_i}^{(i)} = \cos \bar{\varphi}_i \sigma_x^{(i)} + \sin \bar{\varphi}_i \sigma_y^{(i)}$ . The Hamiltonian  $H_D$  acts to displace the position and momentum of the phonon mode  $k$  in a spin-dependent manner by  $\text{Re}(\alpha_k)$  and  $\text{Im}(\alpha_k)$ , respectively, where

$$\alpha_k(t) = \frac{1}{2i} \sum_i \sigma_{\bar{\varphi}_i}^{(i)} \eta_{ik} \int_0^t \Omega_i(t') e^{-i(\delta_k t' + \delta\varphi_i)} dt', \quad (3)$$

as illustrated in Fig. 2. The field amplitude  $\Omega_i(t')$  and relative phase  $\delta\varphi_i(t')$  controls the instantaneous amplitude and direction of displacement at time  $t'$  in the phase space of each mode.

Tuning near the second motional sidebands and denoting the detuning of the laser from the  $k$ th mode by  $\Delta_k \equiv \nu - 2\omega_k$  generates the interaction Hamiltonian under the rotating-wave approximation,

$$H_S = \frac{\hbar}{4} \sum_{k,m,i} \eta_{ik} \eta_{im} \Omega_i(t) e^{\frac{i}{2}(\Delta_k + \Delta_m)t + i\delta\varphi_i} \sigma_{\bar{\varphi}_i}^{(i)} \hat{a}_k \hat{a}_m + \text{h.c.} \quad (4)$$

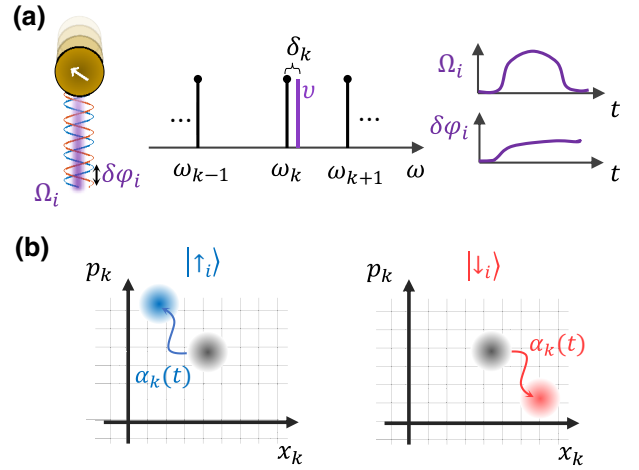


FIG. 2. The state-dependent displacement of motion (displacement Hamiltonian  $H_D$ ). (a) Tuning the frequency  $\nu$  of the drive on the  $i$ th ion near the resonance frequency of the  $k$ th vibrational mode (upper and lower sidebands) couples the spin predominantly with the collective motion of that mode through the displacement Hamiltonian  $H_D$  in Eq. (2). (b) In phase space, the evolution is represented by displacement of the collective ion motion by amount  $\alpha_k$ . The direction of displacement depends on the spin state and is inverted if the  $i$ th spin is flipped. The trajectory  $\alpha_k(t)$  can be temporally engineered via modulation of the field amplitude  $\Omega_i(t)$  and the relative phase  $\delta\varphi_i$  between the upper and lower sideband tones (cf. Eq. (3)). The instantaneous amplitude of motion is controlled by the former, whereas the instantaneous orientation of motion in phase space is controlled by the latter.

This Hamiltonian acts to instantaneously squeeze phase-space coordinates as shown in Fig. 3(a). Here, the relative motional phase between the two tones  $\delta\varphi_i = (\phi_{i+} - \phi_{i-})/2$  determines the axis in which phase-space coordinates are instantaneously squeezed, whereas the common phase  $\bar{\varphi}_i = \pi + (\phi_{i+} + \phi_{i-})/2$  specifies the projection of the spin operator over the Bloch sphere  $\sigma_{\bar{\varphi}_i}^{(i)}$ .

For both displacement and squeezing, we assume that the common phases are fixed during the evolution and set  $\bar{\varphi}_i = \bar{\phi}_i = 0$  such that  $\sigma_{\bar{\varphi}_i}^{(i)} = \sigma_{\bar{\phi}_i}^{(i)} = \sigma_x^{(i)}$ , similar to operation of the MS gate. However, we allow the motional phases  $\delta\varphi_i(t)$  and  $\delta\phi_i(t)$  to vary in time, allowing modulation of the directions of squeezing and displacement during the operation.

Our derivations rely on the Lamb-Dicke approximation, yielding the approximate spin-dependent displacement and spin-dependent squeezing Hamiltonians in Eqs. (2) and (4), respectively. This approximation corresponds to the assumption that the number of phonons in the  $m$ th mode,  $n_m$ , is small (i.e.,  $\eta_{im}\eta_{jm}n_m \ll 1$  for all driven spins  $i, j$  and modes  $m$ ). Breakdown of this approximation can lead to phonon-dependent corrections of the Rabi frequency via the Debye-Waller operator, to breakdown of

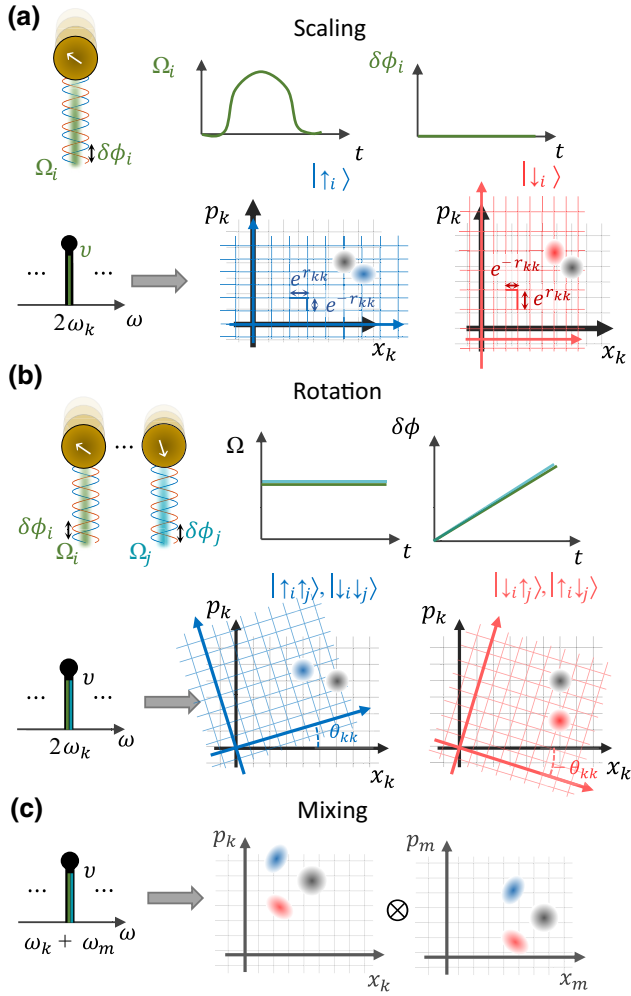


FIG. 3. The state-dependent squeezing of motion (squeezing Hamiltonian  $H_S$ ). Tuning the frequency  $\nu$  of the drive on the  $i$ th ion near twice the resonance frequencies of the vibrational modes generates a spin-dependent coordinate transformation of phase space. (a) The spin-dependent scaling of the phase space of the  $k$ th mode. For  $\nu = 2\omega_k$  and  $\delta\phi = 0$ , the squeezing axis is aligned with the  $\hat{x}_k$  coordinate, resulting in dilation of  $\hat{x}_k$  and contraction of  $\hat{p}_k$  if the spin points upward and vice versa if it points downward. (b) The spin-dependent rotation of the phase space of the  $k$ th mode. Simultaneous modulation of the phase  $\delta\phi$  by an even number of spins results in modulation of the squeezing axis that can effectively rotate phase-space axes. Setting  $\nu = 2\omega_k$  and symmetrically driving spins  $i, j$  can generate a pure spin-dependent rotation, where the axes rotate clockwise if the two spins are aligned and counterclockwise if the spins are antialigned. (c) The spin-dependent mixing of modes. Driving spins synchronously at  $\nu = \omega_k + \omega_m$ , the sum of resonance frequencies of two different modes  $k$  and  $m$  correlate their phase-space coordinates. This correlation is manifested as two-mode squeezing or correlated rotations. Off-resonance driving exerts the interactions in (a)–(c) simultaneously. The spin-dependent scaling matrix  $\mathbf{r}$  and rotation matrix  $\theta$  are uniquely determined by the complex transformation parameters  $\psi$  and  $\chi$  in the main text [see Eqs. (A8) and (A9)].

the rotating-wave approximation, and to other phonon-dependent errors that could limit the realized fidelity [5,51,52]. In practice, this approximation first breaks for phonon modes whose mode participation factors are slowly varying, which efficiently couple to noisy electric fields, resulting in high phonon numbers [53].

### III. EVOLUTION BY THE SQUEEZING HAMILTONIAN

The squeezing Hamiltonian in Eq. (4) contains quadratic motional operators with time-dependent coefficients, generating an infinite series of commutators in the evolution operator. Thus we solve for time evolution of the motional operators in the Heisenberg picture. Since the squeezing Hamiltonian is quadratic in the motional operators, the Heisenberg equations of motion are linear in the same operators and the time evolution can be described by the time-dependent Bogoliubov transformation of the  $k$ th phonon mode:

$$\hat{a}'_k(t) = S_{\psi,\chi}^\dagger(t) \hat{a}_k S_{\psi,\chi}(t) = \sum_{m=1}^M \psi_{km}(t) \hat{a}_m + \chi_{km}(t) \hat{a}_m^\dagger, \quad (5)$$

where  $S_{\psi,\chi}(t)$  is the unitary evolution operator generated by the squeezing Hamiltonian  $H_S$  and  $\hat{a}_k$  is the time-independent annihilation operator in the interaction picture. The transformation in Eq. (5) is complex symplectic [54] and preserves the commutation relations of  $\hat{a}_k$  and  $\hat{a}_k^\dagger$ . It therefore acts to scale, rotate, and mix the phase-space coordinates of the different modes, as we illustrate in Fig. 3 and show in Appendix A.

The transformation at time  $t$  is determined by the complex-valued spin-dependent matrices  $\psi_{km}(t)$  and  $\chi_{km}(t)$ . Differentiation of Eqs. 5 as a function of time yields the dynamics of these matrices via the relations

$$\partial_t \psi_{km} = [\partial_t \hat{a}'_k, \hat{a}_m^\dagger] \quad \text{and} \quad \partial_t \chi_{km}^* = [\hat{a}_m, \partial_t \hat{a}'_k]^*. \quad (6)$$

We can construct the explicit equations of motion for  $\psi_{km}$  and  $\chi_{km}$  by considering the dynamics of the transformed operators  $\hat{a}'_k(t)$  in the Heisenberg picture,

$$\partial_t \hat{a}'_k = S_{\psi,\chi}^\dagger \frac{i}{\hbar} [H_S, \hat{a}_k] S_{\psi,\chi}, \quad (7)$$

where

$$[H_S, \hat{a}_k] = -\hbar \sum_m h_{km} e^{-\frac{i}{2}(\Delta_k + \Delta_m)t} \hat{a}_m^\dagger \quad (8)$$

and

$$h_{km} = \frac{1}{2} \sum_{i=1}^N \eta_{ik} \eta_{im} \Omega_i e^{-i\delta\phi_i} \sigma_x^{(i)}. \quad (9)$$

Substitution of Eqs. (7)–(9) into Eq. (6) and expression of the transformed operators  $\hat{a}'_k(t)$  by the transformation in Eq. (5) yields

$$\partial_t \psi_{km} = -i \sum_l e^{-\frac{i}{2}(\Delta_k + \Delta_l)t} h_{kl} \chi_{lm}^*, \quad (10)$$

$$\partial_t \chi_{km}^* = i \sum_l e^{\frac{i}{2}(\Delta_k + \Delta_l)t} h_{kl}^* \psi_{lm}. \quad (11)$$

Importantly, because of the spin operators in Eq. (9), the transformation parameters  $\psi_{km}(t)$  and  $\chi_{km}(t)$  depend on the many-body spin-state of the  $N \leq M$  ions that are illuminated by the driving fields, rendering an effective  $N$ -body interaction.

For each of the  $2^N$  configurations of these spin states, Eqs. (10) and (11) represent a set of  $N$  linear differential equations with initial conditions  $\psi_{km} = \delta_{km}$  and  $\chi_{km} = 0$ . While the total number of equations scales exponentially in the order of interaction  $N$ , it scales only linearly with the length of the chain  $M$ . The mixing-transformation matrices  $\psi(t)$  and  $\chi(t)$  determine the unitary evolution operator  $S_{\psi, \chi}$  uniquely, as we show in Appendix A. Control over the transformation parameters is thus sufficient to describe the quantum evolution during the squeezing operation.

It is intriguing that the state-dependent transformation that is realized by the squeezing Hamiltonian produces operations, such as state-dependent rotations of phase space, that do not directly appear in the Hamiltonian  $H_S$  in Eq. (4). In fact, the set of effective operations that can be realized belong to the Lie algebra that is generated by this Hamiltonian, which we derive in Appendix B. We find that the group of effective Hamiltonians that can be realized corresponds to the simple symplectic Lie group  $\text{Sp}(2M, \mathbf{R})$  [55] for the motional operators, multiplied by products of spin operators up to order  $N$ . This result is a nontrivial extension of the single-mode case in Refs. [33,39].

#### IV. $N$ -BODY GATE PROTOCOL

We aim to realize a unitary evolution operator that, after some time  $T$ , corresponds to the action of an effective spin Hamiltonian manifesting high-order interactions. As the motional state is prone to heating, dephasing, and initialization errors, high-fidelity manipulation of the spins usually requires the evolution to be insensitive to the initial motional state, as well as the erasure of correlations that are developed between spins and motion during the evolution. This goal underlines a twofold challenge: to engineer useful spin-dependent interactions on one hand and to disentangle the states of motion and spins on the other.

We focus our analysis on a simple protocol that ensures disentanglement of spins and motion at the end of the gate and generates high-order spin interactions independent of

the motional state. The protocol relies on sequential and interleaved applications of squeezing and displacement operations. Independent of the number of ions in the chain  $M$  or the number of target interacting spin bodies  $N$ , we decompose the spin-motion evolution into the following eight stages:

$$U(T) = S_{\psi, \chi}^\dagger D_\beta^\dagger S_{\psi, \chi} D_\alpha^\dagger S_{\psi, \chi}^\dagger D_\beta S_{\psi, \chi} D_\alpha. \quad (12)$$

Here,  $D_\alpha$  and  $D_\beta$  correspond to the displacement evolution operator generated solely by  $H_D$  [Eq. (2)]. We use a vector form of displacement arguments  $\alpha$  and  $\beta$  to compactly denote the target spin-dependent displacements of all modes, with mode  $k$  displaced by the expression in Eq. (3). The term  $S_{\psi, \chi}$  in Eq. (12) corresponds to the squeezing evolution operator generated solely by  $H_S$  [cf. Eq. (4)], with  $\psi$  and  $\chi$  representing the target transformation matrices.

The evolution in Eq. (12) has a simple physical interpretation, which is illustrated graphically in Fig. 4. Absent squeezing operations (i.e.,  $H_S = 0$  and  $S_{\psi, \chi} = \mathbb{1}$ ), the motion of the ions is described by closed contours in phase space of the motional modes, leading to accumulation of a geometric phase  $\Phi_k = 2\text{Im}(\alpha_k^* \beta_k)$  by the  $k$ th phonon mode and thus to a total accumulation of geometric phase  $\Phi = \sum_k \Phi_k$  during the evolution. The spin dependence of this phase gives rise to a quadratic spin Hamiltonian known from the usual MS operation. However, when the squeezing operation  $S_{\psi, \chi}$  is interspersed, it rotates and scales phase-space coordinates, while  $S_{\psi, \chi}^\dagger$  inverts the same. Using Eq. (5), we find that these two squeezing operations generate

$$S_{\psi, \chi}^\dagger D_\beta S_{\psi, \chi} = D_{\beta'}, \quad \text{with } \beta'_k = \sum_m (\psi_{mk}^* \beta_m - \chi_{mk} \beta_m^*). \quad (13)$$

Notably, the resulting evolution has no quadratic terms but, rather, is linear in the motional operators. The emergent displacement vector  $\beta'$  corresponds to displacement by amount  $\beta$  but in a phase space the coordinates of which are scaled or rotated by the transformation matrices  $\psi$  and  $\chi$ . Crucially, the spin dependence of  $\psi$  and  $\chi$  renders  $\beta'$  nonlinear in the spin operators. Therefore, the overall evolution operator  $U$  in Eq. (12) is equivalent to the series of displacements  $\alpha \rightarrow \beta' \rightarrow -\alpha \rightarrow -\beta'$  forming closed contours in phase space and results in an evolution

$$U(T) = e^{-i\Phi} \text{ with } \Phi = 2\text{Im}\left(\sum_k \alpha_k^* \beta'_k\right). \quad (14)$$

Here, the net spin-dependent geometric phase  $\Phi$  is equivalent to the effective spin Hamiltonian

$$H_{\text{eff}} = \hbar\Phi/T, \quad (15)$$

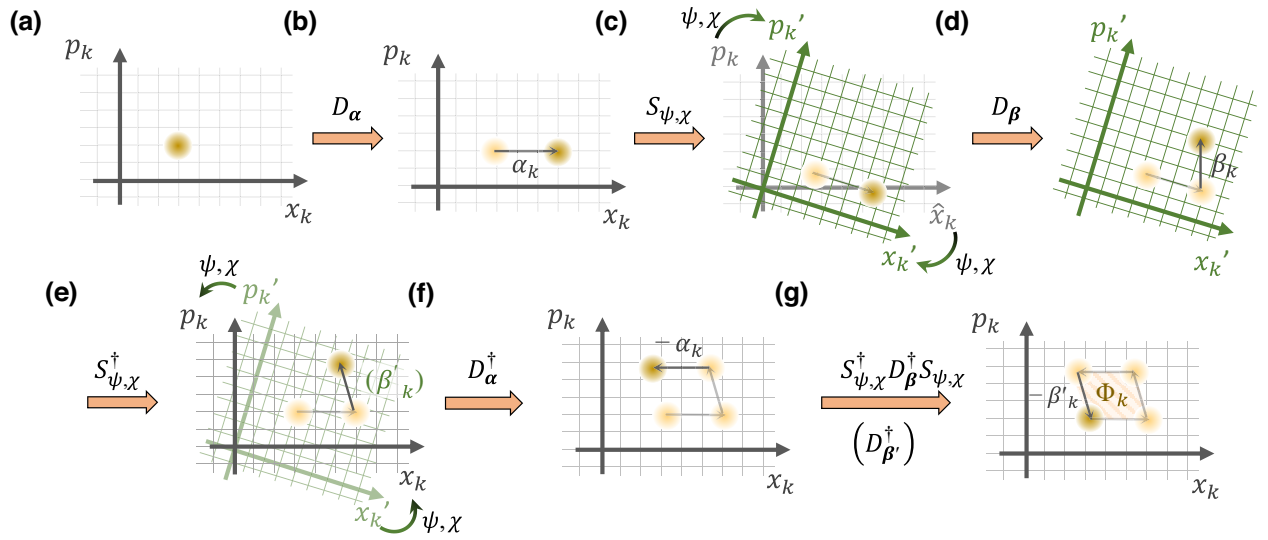


FIG. 4. The protocol for generating high-order spin-dependent Hamiltonians. An illustration of the stages composing the unitary evolution in Eq. (12), constructed by alternate application of the displacement and squeezing operations. (a) The spin state of the ions and the motional state of the crystal is initially decoupled. (b) The displacement of the motion of the  $k$ th vibrational mode by an amount  $\alpha_k$ . (c) The coordinate transformation of phase space with transformation matrices  $\psi$  and  $\chi$  via scaling and rotations generated by the squeezing operation. The motional state remains stationary with respect to the transformed coordinates. (d) The displacement of the ions along the *original coordinate frame* by an amount  $\beta_k$ . (e) Reversal of the coordinate transformation to the original frame in stage (c). The overall evolution in stages (c)–(e) is equivalent to net displacement by an amount  $\beta'_k$  along the transformed reference frame. Importantly, as the coordinate transformation is spin dependent, the transformed displacement  $\beta'_k$  can be comprised of products of multiple spin operators. (f) Reversal of the displacement in (b). (g) Displacement by an amount  $-\beta'_k$  via repetition of the sequence in (c)–(e) but reversal of the evolution in (d). Any entanglement between the spins and motion is erased but the spins accumulate a geometric phase  $\Phi_k$  that is proportional to the area enclosed in phase space. As  $\alpha_k$  and  $\beta'_k$  are spin dependent, so also is  $\Phi_k$ , which corresponds to the effective spin Hamiltonian that is realized by this evolution [cf. Eq. (15)].

where  $T$  is the total duration of the evolution in Eq. (12). The inherent  $N$ -body nature of the evolution operator and Hamiltonian appears in the spin dependencies of  $\alpha_k$ ,  $\beta_k$  and, in particular, the mode-mixing-transformation parameters  $\psi_{km}$  and  $\chi_{km}$ .

## V. APPLICATIONS

In this section, we present two specific sequences for the engineering of particular spin-entangling gates, relying on control over the evolution of all relevant motional modes in the chain. In Sec. V A, we characterize the application of the  $N$ -body stabilizer operator, which is comprised of a product of  $N$  spin operators and is realized via spin-dependent rotation of phase space. In Sec. V B, we investigate a set of Hamiltonians that contain polynomials of spin operators. In Sec. V C, we compare the speed of these implementations with alternative quantum circuits based on concatenation of one- and two-qubit gates. Finally, in Sec. V D we outline a systematic approach for construction of arbitrary high-order spin Hamiltonians. We numerically demonstrate the control fields and characterize the performance of two examples considering a representative chain of 11  $^{171}\text{Yb}^+$  ions in a linear Paul trap, the parameters of which are detailed in Appendix C.

### A. Stabilizer operator

We consider the stabilizer operator

$$\Phi = -\bar{\Phi} \sigma_x^{(i_1)} \otimes \dots \otimes \sigma_x^{(i_N)} \quad (16)$$

as the target effective Hamiltonian in Eq. (15), for an even integer  $N \leq M$ , amplitude  $\bar{\Phi}$ , and a choice of the interacting spins labeled by the vector  $\mathbf{i} = (i_1, \dots, i_N)$ . Notably, the operators in Eq. (16) can be transformed into other operators in the Pauli group via the application of single-qubit gates preceding and following the evolution.

To construct this interaction, we use an alternating sequence of displacements and squeezing from Eq. (12). We consider target displacements of duration  $\tau_d$ , each generated by sequentially illuminating single spins  $i_{N-1}$  and  $i_N$  to produce

$$\alpha_k(\tau_d) = \delta_{kp} A \sigma_x^{(i_{N-1})} \quad \text{and} \quad \beta_k(\tau_d) = i \delta_{kp} B \sigma_x^{(i_N)}, \quad (17)$$

where  $\delta_{kp}$  is the Kronecker delta function. Here, the net phase-space displacement of all modes is ideally zero, except for a particular mode  $p$ . This mode is displaced by magnitude  $A$  along the  $x_p$  coordinate, followed by displacement with magnitude  $B$  along the  $p_p$  coordinate.

Importantly, as the displacements are generated by spin-dependent forces, the sign of  $\alpha_p$  ( $\beta_p$ ) and hence the direction of the displacements depends on the spin state of the  $i_{N-1}$  ( $i_N$ ) ion via the spin operator in Eq. (17).

The other  $N - 2$  spins participate in the desired  $N$ -body stabilizer Hamiltonian via the squeezing operations. We aim for a diagonal mode-mixing transformation matrix at time  $\tau_s$  [33,56], for which

$$\psi_{pp}(\tau_s) = \prod_{n=1}^{N-2} \sigma_x^{(i_n)} = e^{i\frac{\pi}{2} \sum_{n=1}^{N-2} \sigma_x^{(i_n)}} \quad (18)$$

and  $\psi_{kk}(\tau_s) = 1$  for all  $k \neq p$ , with  $\chi_{km}(\tau_s) = 0$  for all modes  $k, m$ . From Eqs. (A8) and (A9), this transformation generates a pure spin-dependent rotation of the phase space

of mode number  $p$  by angle  $\theta_{pp}(\tau_s) = \frac{\pi}{2} \sum_{n=1}^{N-2} \sigma_x^{(i_n)}$ , with no effect on any other mode. The phase space of mode  $p$  is rotated by  $180^\circ$  if  $\frac{1}{2} \sum_{n=1}^{N-2} \sigma_x^{(i_n)}$  is odd and is unaffected if it is even. Substitution of Eqs. (17) and (18) into Eqs. (13) and (14) yields the target stabilizer operator of Eq. (16), with  $\Phi = 2AB$ .

We numerically simulate the operation of this gate, including the effects of all off-resonant modes of motion, with the main results shown in Fig. 5. We generate the wave forms using the optimal-control algorithm GRAPE [57,58] to search for optimal solutions of Eqs. (C4) and (C5) under the target transformation parameters in Eq. (18) (details are given in Appendix C). Here, we generate the desired stabilizer interaction between  $N = 4$  ions in a  $M = 11$  long ion chain. We exemplify a gate acting

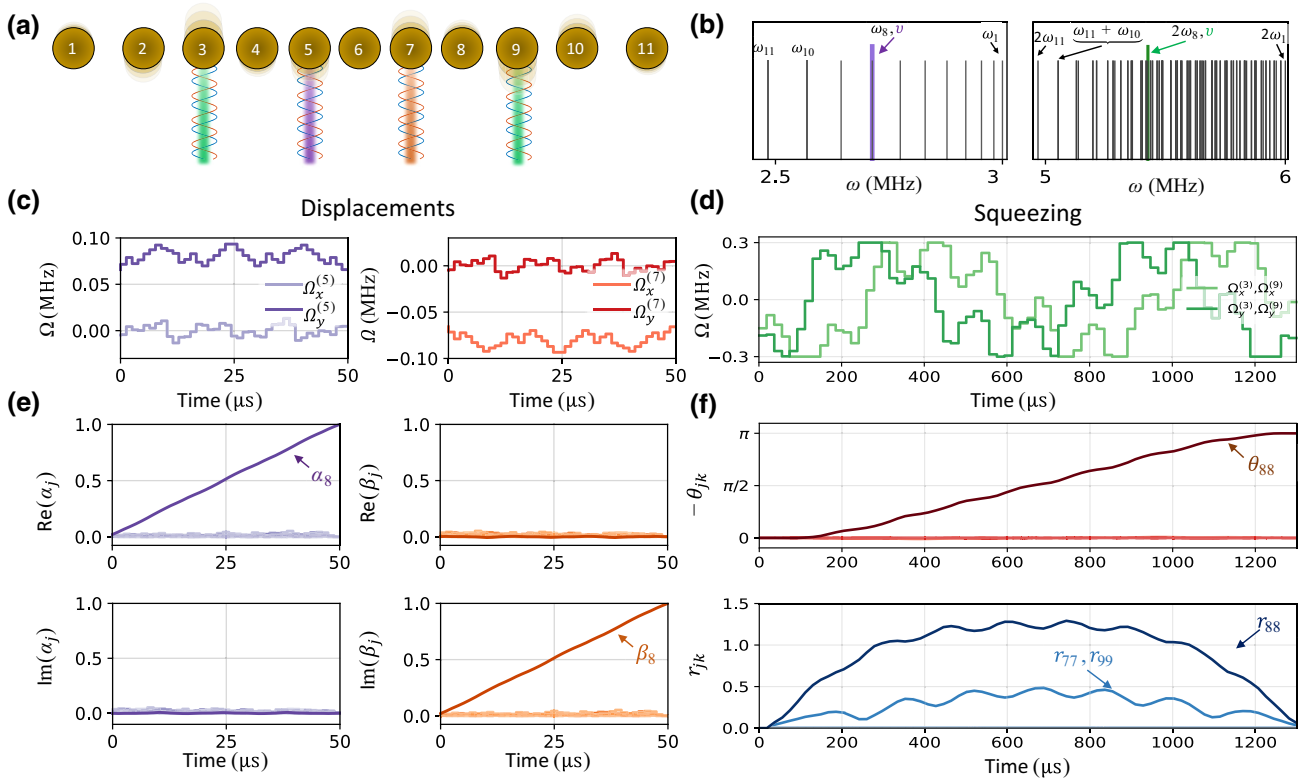


FIG. 5. The numerical implementation of the four-body stabilizer Hamiltonian. (a) Realization of the four-body stabilizer Hamiltonian  $H_{\text{eff}} = \sigma_x^{(3)}\sigma_x^{(9)}\sigma_x^{(5)}\sigma_x^{(7)}$  in a chain of 11 ions based on the protocol in Sec. V A and Eq. (12). We use motional mode  $p = 8$  to generate the interaction, employing ion 5 (7) to displace the position (momentum) of this mode by  $\alpha_8$  ( $\beta_8$ ) and employing ions 3 and 9 to generate pure spin-dependent rotation of phase space via squeezing. (b) The frequency tuning of the displacement and squeezing beams with respect to the first and second sideband transitions, respectively. We use  $\nu = \omega_8$  to generate displacements and  $\nu = 2\omega_8$  to generate squeezing, maximizing the coupling with the desired  $p = 8$  mode. Note that the ions interact with bichromatic fields that symmetrically drive both red and blue sideband transitions but for brevity only the blue sidebands are shown. (c) The calculated phase ( $\Omega_x^{(i)}(t)$ ) and quadrature ( $\Omega_y^{(i)}(t)$ ) components of the control fields, which generate a single displacement over  $\tau_d = 50 \mu$ s by acting on ions  $i = 5, 7$ . (d) The calculated pulse shape (phase and quadrature) of the control fields simultaneously applied to ions  $n = 3, 9$ , which generate rotations over  $\tau_s = 1.3$  ms. We consider simultaneous modulation of  $\Omega_x^{(i)}$  and  $\Omega_y^{(i)}$  for  $i = 3, 9$ . (e),(f) Target displacements and scaling parameters for the spin state  $|\uparrow_x^{(3)}\uparrow_x^{(5)}\uparrow_x^{(7)}\uparrow_x^{(9)}\rangle$ . (e) The target displacements of  $\text{re}(\alpha_8) = 1$  along the  $x_8$  coordinate and  $\text{im}(\beta_8) = 1$  along the  $p_8$  coordinate are realized, while the displacements of all other modes are erased by the end of the pulse. (f) At the end of the sequence, target rotation of  $\theta_{88} = \pi$  inverts the phase-space axes of mode number 8, while the other modes remain invariant. The optimization parameters and the fidelity metrics for this optimization are presented in Appendix C.

on ions  $\mathbf{i} = (3, 5, 7, 9)$  that is mediated predominantly by mode number  $p = 8$ . The frequencies of the beams pointing at ions 5 and 7 are tuned on resonance with the first sidebands of mode 8 ( $\nu = \omega_8$ ;  $\delta_8 = 0$ ) to generate displacement operations, setting  $A = B = 1$  through the control field amplitudes. The beams pointing at the other ions, 3 and 9, are tuned on resonance with the second sidebands of mode 8 ( $\nu = 2\omega_8$ ;  $\Delta_8 = 0$ ) to generate squeezing operations as shown in Fig. 5(b). As expected, the mode spectrum of the second sideband transitions is considerably more crowded owing to nearby intermodulation sidebands between all pairs of modes.

In Figs. 5(c) and 5(d), we present the temporal shape of the control fields using simultaneous amplitude and phase modulation for the displacement pulses  $\tau_d = 50 \mu\text{s}$  [Fig. 5(c)] and for the squeezing pulses [Fig. 5(d)] for  $\tau_s = 1.3 \text{ ms}$ . We express the control field  $\Omega_i(t)$  on each illuminated ion in terms of its quadratures

$$\begin{aligned}\Omega_x^{(i)}(t) &= \Omega_i(t) \sin \mu(t), \\ \Omega_y^{(i)}(t) &= -\Omega_i(t) \cos \mu(t),\end{aligned}\quad (19)$$

with  $\mu(t) = \delta\varphi(t)$  and  $\mu(t) = \delta\phi(t)$  for the displacement and squeezing operations, respectively. We shape the quadrature wave forms  $\Omega_x^{(i)}(t)$  and  $\Omega_y^{(i)}(t)$  during the displacement and squeezing stages using two different optimal-control tools (details are given in Appendix C). We limit the Rabi frequencies  $\Omega_x^{(i)}(t), \Omega_y^{(i)}(t)$  to below 300 KHz to maintain the validity of the rotating-wave approximation.

In Figs. 5(e) and 5(f), we present the outcome phase-space displacements and scaling parameters as a function of time for the particular case in which all spins point upward, resulting in the target evolution. Interestingly for the squeezing evolution, both the target mode and the spectrally nearest modes are squeezed during the pulse, yet disentangle nearly perfectly at the end of the pulse; the numerical optimization over the squeezing-operation wave

forms is terminated when two complementary metrics of infidelity (detailed in Appendix C 3) are lower than 0.1%.

In Fig. 6, we illustrate the spin-dependent evolution in phase space. The spin states of ions 5 and 7 determine the direction of displacement along the position and momentum coordinates of mode  $p = 8$  in phase space, respectively, by setting  $\alpha_8 = A\sigma_x^{(5)}$  and  $\beta_8 = B\sigma_x^{(7)}$ . Application of the target squeezing evolution rotates the phase space of the  $p = 8$  mode in a spin dependent manner, resulting in the modified displacement  $\beta'_8 = \beta_8\sigma_x^{(3)}\sigma_x^{(9)}$ . Consequently, when spins 3 and 9 point along the same direction in their  $x$  basis, the displacement along the momentum coordinate is inverted ( $\beta'_8 = -\beta_8$ ), whereas for spins pointing at the opposite directions, the displacement is unchanged ( $\beta'_8 = \beta_8$ ), therefore resulting in the geometric phase in Eq. (16).

Interestingly, while the number operator  $\hat{a}_8^\dagger\hat{a}_8$  that generates phase-space rotations does not appear in the Hamiltonian in Eq. (4), this operator is generated by sequential application of squeezing operators as discussed in Ref. [59]. The spin-dependent rotation is generated by spin-dependent squeezing operators, such as  $\hat{S}_0 = \sigma_x^{(3)}(\hat{a}_8^2 - \hat{a}_8^{\dagger 2})/2$  (applied when  $\Omega_x^{(3)} \neq 0$ ) and  $\hat{S}_{45} = \sigma_x^{(9)}(\hat{a}_8^2 + \hat{a}_8^{\dagger 2})/2$  (applied when  $\Omega_y^{(9)} \neq 0$ ), the commutation of which yields  $[\hat{S}_0, \hat{S}_{45}] = \sigma_x^{(3)}\sigma_x^{(9)}(\hat{a}_8^\dagger\hat{a}_8 + \frac{1}{2})$  (for further details on the set of operators that can be generated by the evolution, see Appendix B).

## B. $N$ -bit spin polynomials

In Ref. [39], we have proposed the uniaxial squeezing of a single motional mode to generate the target set of effective Hamiltonians

$$H = \frac{\hbar\bar{\Phi}}{T} \prod_{n=1}^N (\mathbb{1} \cosh \xi_n + \sigma_x^{(i_n)} \sinh \xi_n), \quad (20)$$

for  $N \leq M$  and positive and real  $\xi_n$ , where  $\mathbb{1}$  denotes the identity (spin) operator. In the limit  $\xi_n \gtrsim 1$ , the coefficients

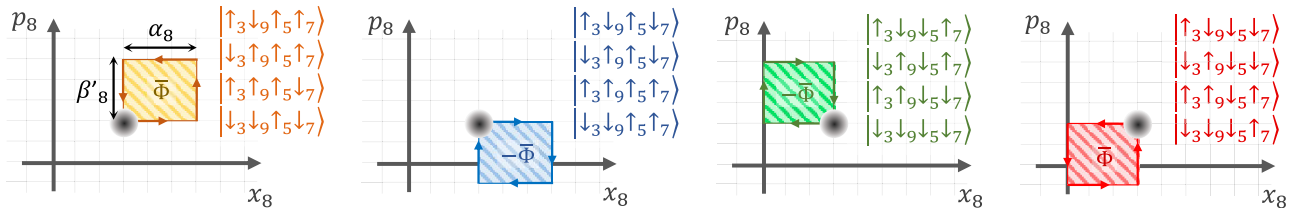


FIG. 6. The phase-space evolution of the stabilizer Hamiltonian. The phase-space trajectories that are used to simulate the evolution of  $U = \exp(-i\bar{\Phi}\sigma_x^{(3)}\sigma_x^{(9)}\sigma_x^{(5)}\sigma_x^{(7)})$  are shown for the 16 different spin states corresponding to the example in Fig. 5, which uses mode number 8. The motion is displaced rightward by  $+\alpha_8$  for  $|\uparrow_5\rangle$  or leftward by  $-\alpha_8$  for  $|\downarrow_5\rangle$ . Similarly, the motion is displaced upward by  $+\beta'_8$  for  $|\uparrow_7\rangle$  or downward by  $-\beta'_8$  for  $|\downarrow_7\rangle$ . Here,  $\beta'_8 = |\beta_8\sigma_x^{(3)}\sigma_x^{(9)}|$  is the displacement generated in the rotated coordinate frame on the state of ions 3 and 9. If ions 3 and 9 are aligned ( $|\uparrow_3\uparrow_9\rangle$  or  $|\downarrow_3\downarrow_9\rangle$ ), then phase space is rotated by  $180^\circ$ , yielding  $\beta'_8 = -|\beta_8|$ , whereas for the antialigned configuration ( $|\uparrow_3\downarrow_9\rangle$  or  $|\downarrow_3\uparrow_9\rangle$ ), phase space is not rotated and  $\beta'_8 = +|\beta_8|$ .

satisfy  $\cosh \xi_n \approx \sinh \xi_n \approx e^{\xi_n}/2$ , and the operator in Eq. (20) becomes a projection operator, which generates the  $N$ -bit controlled-phase gate or the  $N$ -bit Toffoli gate using two additional single-qubit gates.

Here, we extend this approach and analyze the multimode case, which enables the squeezing of a single motional mode in a spin-dependent manner, and we simultaneously erase the undesired evolution that is generated by off-resonant coupling with other modes. Here, we consider the target displacements

$$\alpha_k = \delta_{kp} A \sigma_x^{(\text{aux})} \quad \text{and} \quad \beta_k = i \delta_{kp} B \sigma_x^{(\text{aux})}, \quad (21)$$

which are similar to the displacements in Eq. (17), except that here the two displacements are driven on the same auxiliary spin, which need not appear in the target Hamiltonian and can be any spin in the chain coupled to the involved modes of motion. The coupling between  $N$  spins is then realized via preparing diagonal mode-mixing transformation matrices at time  $\tau_s$  satisfying

$$\psi_{pp}(\tau_s) = \cosh \left( \sum_{n=1}^N \xi_n \sigma_x^{(i_n)} \right) \quad (22)$$

$$\chi_{pp}(\tau_s) = \sinh \left( \sum_{n=1}^N \xi_n \sigma_x^{(i_n)} \right) \quad (23)$$

for a particular target mode  $p$  with all other mode diagonals  $\psi_{kk}(\tau_s) = 1$  and  $\chi_{kk} = 0$ . Substitution of Eqs. (22) and (23) into Eq. (13) reveals that the spin dependence emerges via scaling the displacement along the momentum coordinate of mode  $p$  by  $\beta'_p = \prod_n e^{\sigma_x^{(i_n)} \xi_n} \beta_p$ , which assigns a factor  $e^{\sigma_x^{(i_n)} \xi_n}$  for each spin  $i_n$  that enlarges (compresses) the motion if the  $i_n$  spin points upward (downward).

We demonstrate the operation of this gate in Fig. 7, generating the Hamiltonian in Eq. (20) between  $N = 4$  ions for an  $M = 11$  ion chain and for the target parameters  $\xi_n = 0.325$ . We demonstrate the interaction between ions 4, 5, 7, and 8 mediated predominantly by mode number  $p = 10$ . The four ions are driven by beams that are tuned at  $\nu = 2\omega_{10}$  for  $\tau_s = 200 \mu\text{s}$  and the control fields are presented in Fig. 7(b). This pulse acts to squeeze mode  $p = 10$  by a factor  $e^{r_{10,10}}$  and to disentangle the effect over all other modes, as presented for the case in which all the spins point upward in Fig. 7(c). For the displacements, we use ion number 3 as the auxiliary ion.

### C. Comparison with one- and two-qubit gate implementations

The trapped-ion processor can be used as a universal quantum computer to alternatively express the  $N$ -body phase gates in Eqs. (16) and (20) as a concatenation of one- and two-qubit gates. In this subsection, we consider this

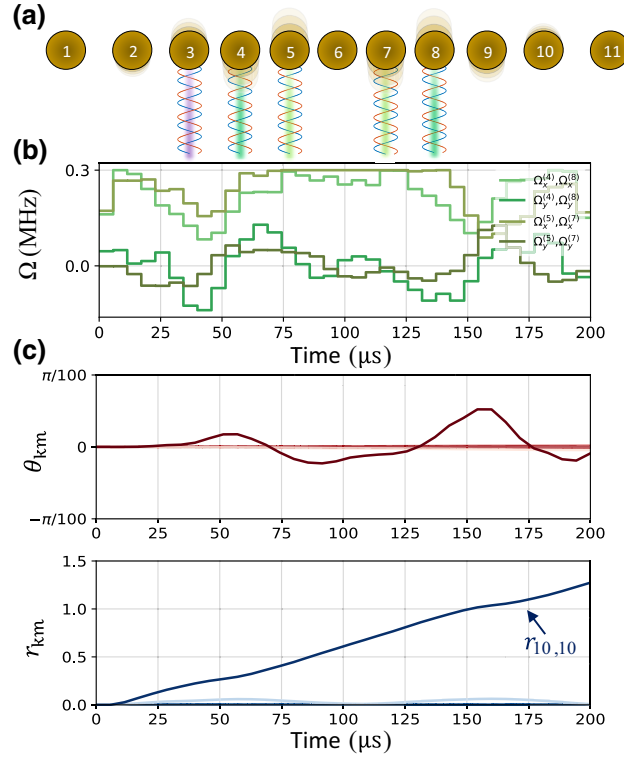


FIG. 7. The numerical implementation of a four-body spin-polynomial Hamiltonian. We exemplify the realization of a target four-body Hamiltonian  $H_{\text{eff}} = (a\mathbb{1} + b\sigma_x^{(4)})(a\mathbb{1} + b\sigma_x^{(5)})(a\mathbb{1} + b\sigma_x^{(7)})(a\mathbb{1} + b\sigma_x^{(8)})$  with  $a \approx 1.053$  and  $b \approx 0.331$  in a chain of 11 ions. (a) We drive ions 4, 5, 7, and 8 with the squeezing interaction resonant with mode number  $p = 10$  and use ion 3 as an auxiliary ion to generate displacement in that mode. (b) The calculated pulse shape of the control fields for the squeezing interaction with  $\tau_s = 200 \mu\text{s}$ . Here, the four spins are driven predominantly by  $\Omega_x^{(i)}$ , which squeezes the axes along the  $\hat{x}_{10}$  coordinate. By symmetry of that mode, the optimal-control fields for ions  $i = 4, 8$  as well as for ions  $i = 5, 7$  are identical. (c) The target scaling parameters for the spin state  $|\uparrow_x^{(4)} \uparrow_x^{(5)} \uparrow_x^{(7)} \uparrow_x^{(8)}\rangle$ . Target exponential scaling of  $r_{10,10} = 2$  squeezes  $\hat{x}_{10}$  and anti-squeezes  $\hat{p}_{10}$  while erasing mixing, rotations, and squeezing of all other modes by the end of the pulse. The realized displacements and control fields for this case are qualitatively similar to those presented in Fig. 5. The optimization parameters and the fidelity metrics for this optimization are presented in Appendix C.

approach to the four-qubit gates in Secs. VA and VB and highlight the conditions under which the proposed  $N$ -body gates are expected to improve the run time.

We decompose the  $N$ -body gates into quantum circuits using protocols in Refs. [60–62], employing a native gate set composed of one-qubit rotation operations  $R(\theta, \phi)$  with polar angle  $\theta$  and azimuthal angle  $\phi$  together with controlled-NOT (CNOT) gates as two-qubit gates. We further improve our construction by using QISKIT transpiler [63] and present the equivalent four-qubit stabilizer and polynomial phase gate circuits in Appendix D. The four-qubit

stabilizer gate in Sec. VA requires six two-qubit gates and the polynomial gate in Sec. VB requires 16 two-qubit gates, in addition to several single-qubit gates (which, for simplicity, we disregard in this analysis). Assuming a typical time of 100–200  $\mu\text{s}$  per (serial) two-qubit gate for chains of  $^{171}\text{Yb}^+$  hyperfine qubits [42,64–67], the stabilizer gate is expected to require 1 ms and the polynomial gate of approximately 2.5 ms. In comparison, the protocols in Secs. VA and VB require about 5.5 ms and 1 ms for these two gates, respectively. We therefore expect that, in this example, the effective polynomial gate can outperform the quantum circuit in run time, while the stabilizer gate is likely to fall behind.

The difference in the number of two-qubit operations between the stabilizer and the polynomial gates is related to the number of Pauli strings in the effective Hamiltonian. We consider Pauli string operators of the form  $P(q_1, \dots, q_N) = \prod_{i=1}^N s_q^{(i)}$  for  $q_i \in \{0, 1\}$ , with  $s_0^{(i)} = \mathbb{1}_\sigma^{(i)}$  as the identity operator of the  $i$ th qubit and  $s_1^{(i)} = \sigma_x^{(i)}$ . A Hamiltonian composed of a single Pauli string, such as the one corresponding to the stabilizer gate in Sec. VA, can be constructed by applying multiple two-qubit operations, with the number of operations scaling linearly with  $N$  [61,62]. General polynomial gates, expressed as diagonal unitary matrices using  $x$  as the quantization axis, require a larger number of Pauli string operators that, in the worst case, could scale exponentially with the number of qubits [60,68]. The speed of squeezing operations on the other hand, is limited by the typical frequency spacing of the second-sideband spectrum and, for a fixed laser power, scales as the square of the Lamb-Dicke parameters; it is typically inversely proportional to the number  $M$  of total qubits and is fixed for a given number of ions. Because squeezing-based gates allow for implementation of a family of many Pauli strings in a single sequence of squeezing and displacement operations (which does not scale with the number  $N$  of involved qubits), we expect that their speed could outperform standard circuit techniques for large  $N$  and for gates consisting of numerous Pauli strings.

The exact transition point in the efficiency of the two methods depends on the target gate and also on the experimental configuration. In this analysis, we consider relatively small Lamb-Dicke parameters  $\eta_{i,k} \approx 0.1 b_{ik}$  associated with driving the clock hyperfine states of  $^{171}\text{Yb}^+$  ions using the Raman interaction (for exact values, see Appendix C). This renders the squeezing operations slow, compared with the displacement operations that generate two-qubit gates. Notably, lighter-mass ions can achieve considerably higher Lamb-Dicke parameters [69] and can potentially further speed up gates based on spin-dependent squeezing. In summary, the direct comparison between these two classes of quantum circuits and/or gates will depend highly upon the higher-level structure of a larger quantum circuit.

## D. High-order spin Hamiltonians

The applications in Secs. VA and VB are based on spin-dependent coordinate transformations of a *single* motional mode and the successful disentanglement of all other modes from the transformation. One strategy for generating other high-order Hamiltonians in a single step is to decompose a target spin Hamiltonian into  $m \leq M$  spin-polynomials, the structure of which is similar to that of Eqs. (16) and (20). Then, each term can be assigned to a different motional mode and the control fields for the target displacements and scaling parameters can be calculated in parallel, similar to the way in which parallel Mølmer-Sørensen gates are constructed [70,71].

## VI. DISCUSSION AND CONCLUSIONS

The use of spin-dependent squeezing operations between trapped atomic ion spins is a powerful technique for generating a variety of many-body interactions. By driving transitions near the first and second sideband spectrum, the resulting spin-dependent displacement and squeezing operations conspire to form families of spin-entangling gates that implement interaction between  $N$  bodies, while being robust to thermal motion of the ions. We derive the Heisenberg equations of motion that enable to shape the optical fields to achieve the desired evolution over all motional modes, including those off resonance from the targeted sidebands. Finally, we numerically demonstrate and analyze the operation of two different gate families in an 11-ion chain.

Interestingly, the spin-dependent squeezing Hamiltonian, the terms of which are quadratic in the motional creation and annihilation operators, allows displacement operations with a linear spin dependence to produce nonlinear spin interactions. Our representation of the squeezing action as a spin-dependent coordinate transformation reveals the origin of this nonlinearity: while the rotation angle and the squeezing parameter depend linearly on the spins, the squeezing and rotation change the motional coordinates and the underlying geometrical phase in a nonlinear manner.

Remarkably, controllable interactions can be realized despite the complex structure of the Hamiltonian. While the Magnus expansion [1,70,72,73] or the Wei-Norman factorization [5,39,74] provide a description of unitary evolution under time-dependent displacement Hamiltonians, these techniques are not suitable for describing the action of the time-dependent squeezing Hamiltonian with more than one motional mode, owing to the nonterminating commutation relation of quadratic bosonic Hamiltonians. In contrast, using the time-dependent coordinate transformation in the Heisenberg picture uniquely determines the unitary evolution and, importantly, renders the control problem tractable, where the number of equations,

for a given order of interaction, scales linearly with the number of ions in the chain. This allows the design of pulses that disentangle the spins from the motional state at the end of the gate, thus erasing any squeezing, rotations, and intermode mixing of the motional modes that are generated during the gate. Owing to the frequency selectivity of the modes, this can be done despite the dense mode spectrum of the second sidebands and the presence of the intermode coupling terms in the Hamiltonians.

The analysis in this work focuses on a simple protocol, which demonstrates the construction of high-order spin-spin interactions and the disentanglement of spin and motion degrees of freedom. Noisy control fields are expected to generate errors in the unitary evolution of both the displacement and squeezing operations, affecting the overall gate fidelity. We expect that the present protocol can be extended and optimized for robust performance in the presence of noisy control fields, reminiscent of protocols that optimize for the robustness of MS pairwise gates under noisy control fields [9–11,75].

For practical applications, it is possible to further speed up the gates by increasing the Rabi frequencies during the squeezing operation ( $\Omega_i \lesssim \omega_k$ ). This requires the consideration of fast-rotating terms that can no longer be neglected in the rotating-wave approximation. At these Rabi frequencies, the displacement and squeezing Hamiltonians are accompanied by additional terms, including off-resonant coupling to the carrier transition and the first-sideband spectrum. Off-resonant driving of the carrier transition results in a one-body spin Hamiltonian that commutes with  $H_S$  and can be compensated at the end of the circuit via additional single-qubit gates. Off-resonant driving of the first sideband transitions results in a spin-dependent displacement Hamiltonian. Owing to the large detuning, its action is akin to the regime used by quantum simulators [1]; it leads to pairwise Ising interactions between the driven spins and to very small spin-flip error that scales as  $\sum_k (\eta_{ik} \Omega_i / \delta_k)^2$  for the  $i$ th ion. The Ising interactions can be suppressed by simultaneous application of the displacement Hamiltonian with additional tones or by Hamiltonian-engineering techniques [76,77].

$N$ -body interactions between trapped neutral atoms or ions have also been proposed in other architectures, using, e.g., trap-mediated Rydberg interactions [78,79]. These proposals operate in the dispersive regime, maintain a nonzero spin-phonon entanglement [8], and are natively limited to coupling between neighboring atoms unless the trapping potential is shaped to soften the motional modes. The proposal in this work, akin to MS gates, is not limited to operation in the dispersive regime, nor to a particular trapping potential. It might therefore be beneficial for digital quantum computation applications that harness control over the radiation fields to disentangle spins and phonons and benefit from dense and nonlocal connectivity between the spins.

This work paves the way toward efficient realization of complex building blocks for quantum computations and simulations in trapped-ion systems. The tools and concepts developed in this work might also find use in other contexts. For example, they might have applications in continuous-variable quantum information applications [80–87] or in other physical systems manifesting coupling between spins and bosonic modes that act as a quantum bus, such as in superconducting circuits embedded in microwave cavities or arrays of neutral atoms in optical cavities.

## ACKNOWLEDGMENTS

This work is supported by the Army Research Office (ARO) through the Intelligence Advanced Research Projects Activity (IARPA) Logical Qubits (LogiQ) program; the National Science Foundation (NSF) Software-Tailored Architecture for Quantum Co-design (STAQ) and Quantum Leap Challenge Institute programs; the U.S. Department of Energy (DOE) Quantum Systems Accelerator (QSA) program; the Air Force Office of Scientific Research (AFOSR) Multidisciplinary Research Programs of the University Research Initiative (MURIs) on Dissipation Engineering in Open Quantum Systems, Quantum Measurement/Verification, and Quantum Interactive Protocols; the ARO MURI on Modular Quantum Circuits; and by the DOE High Energy Physics (HEP) Quantum Information Science Enabled Discovery (QuantISED) program through the GeoFlow Grant No. de-sc0019380.

## APPENDIX A: SQUEEZING OPERATION AS COORDINATE TRANSFORMATION IN PHASE SPACE

We can interpret the Bogoliubov transformation in Eq. (5) via the simple transformation  $\hat{a}'_k = \hat{x}'_k + i\hat{p}'_k = S_{\psi,\chi}^\dagger \hat{a} S_{\psi,\chi}$ , where  $\hat{x}'_k$  and  $\hat{p}'_k$  are the dimensionless quadratures used to illustrate phase space in all figures. Then, the equivalent transformation of these phase-space operators in the Heisenberg picture reads

$$\hat{x}'_k(t) = \sum_{m=1}^M \lambda_{km}(t) \hat{x}_m + \lambda_{k\tilde{m}}(t) \hat{p}_m, \quad (\text{A1})$$

$$\hat{p}'_k(t) = \sum_{m=1}^M \lambda_{\tilde{k}m}(t) \hat{x}_m + \lambda_{\tilde{k}\tilde{m}}(t) \hat{p}_m, \quad (\text{A2})$$

where  $\tilde{k} = k + M$  and  $\tilde{m} = m + M$  for brevity. The transformation matrix  $\lambda(t)$  of size  $2M \times 2M$  is a function of  $\psi$  and  $\chi$  that is given by

$$\lambda_{mk} = \text{Re}(\psi_{mk} + \chi_{mk}) \quad \text{and} \quad \lambda_{\tilde{m}\tilde{k}} = \text{Re}(\psi_{mk} - \chi_{mk}), \quad (\text{A3})$$

$$\lambda_{\bar{m}k} = \text{Im}(\psi_{mk} + \chi_{mk}) \quad \text{and} \quad \lambda_{m\bar{k}} = \text{Im}(\chi_{mk} - \psi_{mk}). \quad (\text{A4})$$

It preserves the commutation relations of  $\hat{x}_k$  and  $\hat{p}_k$  at any time and mathematically corresponds to a linear symplectic transformation. It therefore acts to scale, rotate, and mix the different phase-space coordinates, as we illustrate in Fig. 3. The components  $\lambda_{kk}$  and  $\lambda_{\bar{k}\bar{k}} \neq 1$  change the scaling of the coordinates of the  $k$ th mode in phase space and the components  $\lambda_{\bar{k}\bar{k}}$  and  $\lambda_{\bar{k}\bar{k}} \neq 0$  correspond to their rotation. All other components correspond to correlated mixing of the different modes:  $\lambda_{km}$  and  $\lambda_{\bar{k}\bar{m}} \neq 0$  mix the coordinates of two different modes  $m \neq k$  in the form of correlated scaling (i.e., via two-mode squeezing) and  $\lambda_{k\bar{m}}$  and  $\lambda_{\bar{k}m} \neq 0$  mix the two modes via correlated rotations (i.e., by exchange of phonons between the modes).

We now discuss a specific representation of the coordinate transformation defined by  $\psi$  and  $\chi$  and show how they determine the evolution operator  $S_{\psi,\chi}$ . The representation we use supports the simple physical interpretation of scaling and rotation of phase space by the end of the squeezing evolution at time  $\tau_s$ . Based on the polar decomposition carried in Refs. [54,88], the complex scaling-parameters at a given time  $t$  can be represented by

$$\psi_{km}(t) = (\cosh \mathbf{r} e^{i\theta})_{km}, \quad (\text{A5})$$

$$\chi_{km}(t) = (\sinh \mathbf{r} e^{i\theta} e^{-i\theta^T})_{km}, \quad (\text{A6})$$

where  $\mathbf{r}(t)$ ,  $\boldsymbol{\vartheta}(t)$ , and  $\boldsymbol{\theta}(t)$  are Hermitian,  $M \times M$  matrices and  $1 \leq m, k \leq M$ .  $\mathbf{r}(t)$  is a positive semidefinite matrix that describes the degree of squeezing of phase space at time  $t$ ,  $\boldsymbol{\vartheta}(t)$  describes the axes of squeezing in phase space at time  $t$ , and  $\boldsymbol{\theta}(t)$  describes all phase-space rotations at time  $t$ . The roles of these different matrices can also be seen via explicit representation of the evolution operator by [89]

$$S_{\psi,\chi} = e^{\frac{1}{2} \sum_{mk} (\hat{a}_m^\dagger \hat{a}_k^\dagger z_{mk} - \hat{a}_m \hat{a}_k z_{mk}^\dagger)} e^{i \sum_{mk} \theta_{mk} \hat{a}_m^\dagger \hat{a}_k}, \quad (\text{A7})$$

where  $\mathbf{z}(t) = \mathbf{r} e^{i\theta}$  is a symmetric matrix that represents the multimode squeezing in a polar form. The first exponential map in Eq. (A7) is the multimode squeezing operator, which mixes and scales the phase spaces of the modes, and the second exponential term is a beam-splitter term, which rotates and mixes phase space. The representation in Eq. (A7) uniquely determines the evolution operator, which establishes a relation to the transformation parameters via Eqs. (A5) and (A6) by

$$\mathbf{r} = \log \left( \sqrt{\psi \psi^\dagger} + \sqrt{\chi \chi^\dagger} \right), \quad (\text{A8})$$

$$\boldsymbol{\theta} = -i \log \left( \left( \sqrt{\psi \psi^\dagger} \right)^{-1} \psi \right), \quad (\text{A9})$$

where all operations including  $\log()$  and  $\sqrt{\phantom{x}}$  are full matrix operations. Equation (A9) is derived by inverting Eq. (A5) as  $e^{i\theta} = (\cosh \mathbf{r})^{-1} \psi$  and using  $(\cosh \mathbf{r})^2 = \psi \psi^\dagger$ . For other representations of  $S_{\psi,\chi}$ , see Refs. [90,91].

It is insightful to consider the values of the transformation  $\lambda(\tau_s)$  for some particular sets of target values. Specifically, we consider cases for which the target matrices  $\mathbf{r}(\tau_s)$  and  $\boldsymbol{\theta}(\tau_s)$  are nearly diagonal and for  $\boldsymbol{\vartheta}(\tau_s)$  that is nearly the zero matrix. The former condition minimizes the mixing between different modes by the squeezing interaction, whereas the latter condition aligns the squeezing and antisqueezing axes to be predominantly along the  $\hat{x}_k$  and  $\hat{p}_k$  coordinates in all  $1 \leq k \leq M$  phase spaces. Under these conditions, the transformation matrix is given to zeroth order by

$$\begin{pmatrix} \lambda_{mm} & \lambda_{m\bar{m}} \\ \lambda_{\bar{m}m} & \lambda_{\bar{m}\bar{m}} \end{pmatrix} \approx \begin{pmatrix} e^{r_{mm}} & 0 \\ 0 & e^{-r_{mm}} \end{pmatrix} \times \begin{pmatrix} \cos \theta_{mm} & -\sin \theta_{mm} \\ \sin \theta_{mm} & \cos \theta_{mm} \end{pmatrix}, \quad (\text{A10})$$

where all other  $m \neq k$  coefficients are small:

$$\lambda_{mk}, \lambda_{m\bar{k}}, \lambda_{\bar{m}k}, \lambda_{\bar{m}\bar{k}} \ll 1. \quad (\text{A11})$$

In this representation, the phase-space coordinates transform by a two-stage process. First, the  $\hat{x}_m$  and  $\hat{p}_m$  coordinates of the  $m$ th mode are rotated by an angle  $\theta_{mm}$ . Then, the rotated coordinates are scaled by a factor  $e^{r_{mm}}$  along the rotated  $\hat{x}_m$  and by a factor  $e^{-r_{mm}}$  along the rotated  $\hat{p}_m$ .

## APPENDIX B: THE REACHABLE SET OF EFFECTIVE HAMILTONIANS

In this appendix, we construct the Lie algebra  $L$ , the elements of which compose the reachable set of effective time-independent Hamiltonians that can be realized by the time-dependent Hamiltonian  $H_S + H_D$ . This set is constructed by repeated application of the commutator operation over the operators appearing in the Hamiltonian. First, we construct the elements of the simple Lie algebra span( $\mathcal{S}$ ) that is associated with the squeezing Hamiltonian. We do so by commuting the operators that appear only in the squeezing Hamiltonian. This Hamiltonian contains the set of operators

$$\mathcal{S}_1 = \{ \mathfrak{s}_i^{(1)} (\hat{a}_m^2 \pm \hat{a}_m^{\dagger 2}), \mathfrak{s}_i^{(1)} (\hat{a}_m \hat{a}_k \pm \hat{a}_m^\dagger \hat{a}_k^\dagger) \} \quad (\text{B1})$$

for  $1 \leq k, m \leq M$  and  $m \neq k$ , where  $\mathfrak{s}_i^{(1)} = \sigma_x^{(i_1)}$  and  $1 \leq i_1 \leq M$ . The operator  $\mathfrak{s}_i^{(n)}$  compactly denotes a product of  $n$  spin operators by

$$\mathfrak{s}_i^{(n)} = \sigma_x^{(i_1)} \otimes \dots \otimes \sigma_x^{(i_n)}, \quad (\text{B2})$$

where the vector  $\mathbf{i} = (i_1, \dots, i_n)$  indexes all possible spin combinations that appear in the product via  $0 \leq n \leq M$ .

Using the bosonic commutation relations  $[\hat{a}_m, \hat{a}_k^\dagger] = \delta_{mk}$  and  $[\hat{a}_m, \hat{a}_k] = 0$  and the identities

$$[\hat{a}_m^2, \hat{a}_m^{\dagger 2}] = 4\hat{a}_m^\dagger \hat{a}_m + \frac{1}{2} \quad \text{and} \quad [\hat{a}_m \hat{a}_k, \hat{a}_m^{\dagger 2}] = 2\hat{a}_m^\dagger \hat{a}_k, \quad (\text{B3})$$

by commuting the terms in  $\mathcal{S}_1$  we find the linearly independent set of operators

$$\mathcal{S}_2 = \{\mathfrak{s}_i^{(2)}(\hat{a}_m^\dagger \hat{a}_m + \frac{1}{2}), \mathfrak{s}_i^{(2)}(\hat{a}_m^\dagger \hat{a}_k \pm \hat{a}_m \hat{a}_k^\dagger)\}, \quad (\text{B4})$$

where  $\mathfrak{s}_i^{(2)} = \sigma_x^{(i_1)} \sigma_x^{(i_2)}$  and  $1 \leq i_1, i_2 \leq M$ . Commutation of the different terms in  $\mathcal{S}_1$  with the terms in  $\mathcal{S}_2$  and use of the identities

$$\begin{aligned} [\hat{a}_m^2 \pm \hat{a}_m^{\dagger 2}, \hat{a}_m^\dagger \hat{a}_m] &= 2(\hat{a}_m^2 \mp \hat{a}_m^{\dagger 2}) \quad \text{and} \\ [\hat{a}_m \hat{a}_k^\dagger, \hat{a}_m^{\dagger 2}] &= 2\hat{a}_m^\dagger \hat{a}_k^\dagger, \end{aligned} \quad (\text{B5})$$

yields the linearly independent set of operators

$$\mathcal{S}_3 = \{\mathfrak{s}_i^{(3)}(\hat{a}_m^2 \pm \hat{a}_m^{\dagger 2}), \mathfrak{s}_i^{(3)}(\hat{a}_m \hat{a}_k \pm \hat{a}_m^\dagger \hat{a}_k^\dagger)\}, \quad (\text{B6})$$

where  $\mathfrak{s}_i^{(3)} = \sigma_x^{(i_1)} \sigma_x^{(i_2)} \sigma_x^{(i_3)}$  and  $1 \leq i_1, i_2, i_3 \leq M$ . Similarly, commutation of the terms  $\mathcal{S}_1$  with the terms in  $\mathcal{S}_3$  as well as commutation of terms in  $\mathcal{S}_2$  with terms in  $\mathcal{S}_3$  yields the set of operators

$$\mathcal{S}_4\{\mathfrak{s}_i^{(4)}(\hat{a}_m^\dagger \hat{a}_m + \frac{1}{2}), \mathfrak{s}_i^{(4)}(\hat{a}_m^\dagger \hat{a}_k \pm \hat{a}_m \hat{a}_k^\dagger)\}, \quad (\text{B7})$$

where  $\mathfrak{s}_i^{(4)} = \sigma_x^{(i_1)} \sigma_x^{(i_2)} \sigma_x^{(i_3)} \sigma_x^{(i_4)}$  and  $1 \leq i_1, i_2, i_3, i_4 \leq M$ . It is therefore evident that for every  $\mathcal{S}_n$  that is constructed by  $n - 1$  commutations of the terms in  $\mathcal{S}_1$ , the motional operators would maintain their quadratic form and be multiplied by a product of  $n$  spin operators. The set  $\mathcal{S}$  is then constructed by

$$\mathcal{S} = \mathcal{S}_1 \cup \dots \cup \mathcal{S}_M, \quad (\text{B8})$$

which yields

$$\mathcal{S} = \{\hat{a}_k \hat{a}_m \mathfrak{s}_i^{(n_o)}, \hat{a}_k^\dagger \hat{a}_m^\dagger \mathfrak{s}_i^{(n_e)}, (\hat{a}_k^\dagger \hat{a}_m + \frac{1}{2} \delta_{mk}) \mathfrak{s}_i^{(n_e)}\}, \quad (\text{B9})$$

where  $n_o$  ( $n_e$ ) run over all odd (even) values of  $n$ . Mathematically, if we consider the set along an eigenstate of the spin operators, then  $\mathcal{S}$  corresponds to the simple Lie group  $\text{Sp}(2M, \mathbf{R})$  [55].

Interestingly,  $\mathcal{S}$  extends the set of operators that directly appear in the Hamiltonian  $H_S$ , introducing new spin-motion terms in the unitary evolution. From the spin sector, the squeezing interaction generates products of  $n > 1$  spin operators, whereas  $H_S$  contains a *single* spin operator ( $n = 1$  in Eq. (B2)). From the motional sector, new terms that are proportional to  $(\hat{a}_k^\dagger \hat{a}_m + \frac{1}{2} \delta_{mk})$  appear, which act to rotate

the phase-space coordinates as visualized in Fig. 3. However, as the quadratic dependence of the motional operators in  $\mathcal{S}$  is preserved, the motional identity  $\mathbb{1}$  that can be associated with a motion-independent effective Hamiltonian is not generated.

The Lie algebra associated with the total displacement and squeezing Hamiltonian is given by  $L = \text{span}(\mathcal{S} \cup \mathcal{D})$ . To construct the operators in  $\mathcal{D}$ , we first identify the operators that are generated solely by the displacement Hamiltonian corresponding to the sets

$$\mathcal{D}_1 = \{\mathfrak{s}_i^{(1)} \hat{a}_k, \mathfrak{s}_i^{(1)} \hat{a}_k^\dagger\} \quad \text{and} \quad \mathcal{D}_2 = \{\mathfrak{s}_i^{(2)}\}, \quad (\text{B10})$$

where  $\mathcal{D}_1$  corresponds to the linearly independent set of operators appearing in  $H_D$  and  $\mathcal{D}_2$  is generated by commutation of the elements in  $\mathcal{D}_1$ . As the terms in  $\mathcal{D}_2$  trivially commute, absent the squeezing interaction  $\mathcal{D}_{\text{MS}} = \mathcal{D}_1 \cup \mathcal{D}_2$  manifests the reachable set by the MS-type interaction, corresponding to motional displacements that are linear in the spin operators and pairwise spin-spin interactions.

With the introduction of the squeezing Hamiltonian, this reachable set can be further extended. Using the simple commutation relations  $[\hat{a}_k^2, \hat{a}_k^\dagger] = 2\hat{a}_k$  and  $[\hat{a}_k^{\dagger 2}, \hat{a}_k] = -2\hat{a}_k^\dagger$ , we can commute the terms in  $\mathcal{D}_1$  with the terms in  $\mathcal{S}_1$  for  $n \geq 1$  times and by that construct the sets  $\tilde{\mathcal{D}}_n = \{\mathfrak{s}_i^{(n+1)} \hat{a}_k, \mathfrak{s}_i^{(n+1)} \hat{a}_k^\dagger\}$ . Further commutation of these sets yields the motion-independent set  $\tilde{\mathcal{D}}_0 = \{\mathfrak{s}_i^{(j)} | 1 \leq j \leq M\}$ . These sets can finally be united to construct

$$\mathcal{D} = \tilde{\mathcal{D}}_0 \cup \tilde{\mathcal{D}}_1 \cup \dots \cup \tilde{\mathcal{D}}_{M-1}, \quad (\text{B11})$$

which corresponds to

$$\mathcal{D} = \{\hat{a}_k \mathfrak{s}_i^{(n)}, \hat{a}_k^\dagger \mathfrak{s}_i^{(n)}, \mathbb{1} \mathfrak{s}_i^{(n)}\}, \quad (\text{B12})$$

thus containing the target  $n$ -body terms  $\mathbb{1} \mathfrak{s}_i^{(n)}$  that we aim to generate.

## APPENDIX C: NUMERICAL IMPLEMENTATION OF OPTIMAL-CONTROL SOLVER

In this appendix, we describe the optimal-control tools used to compute the control fields for the displacement and squeezing operations in Sec. V. We first describe the system parameters for which the calculation is demonstrated. We consider a linear chain of 11 ions in a quadratic potential. We assume the single ion axial and secular radial frequencies  $\omega_z = 0.39$  MHz and  $\omega_r = 3$  MHz, which determine the positions of the ions, the mode spectrum, and the mode participation factors. We order the radial modes that are used for coupling the ions in a decreasing order, corresponding to the ordered set of frequencies  $\omega_k \in \{3, 2.981, 2.954, 2.919, 2.878, 2.830, 2.775, 2.713, 2.645, 2.569, 2.484\}$  MHz for  $1 \leq k \leq 11$ . We assume a single-ion Lamb-Dicke parameter of  $\eta \equiv \delta K \sqrt{\hbar/2M\omega_r} = 0.1$

for the driving field and that the bichromatic field couples to the modes along a single radial axis. We also limit the drive-field amplitude quadratures of each ion,  $\Omega_x^{(i)}$  and  $\Omega_y^{(i)}$ , to be  $\lesssim 0.3$  MHz.

### 1. optimal control of spin-dependent displacements

We use a simple optimal-control tool to calculate the control fields  $\Omega_x^{(i)}(t)$  and  $\Omega_y^{(i)}(t)$  for a specific ion  $i$  given a target displacements vector  $\alpha(\tau_d)$ . Standard optimization tools that calculate the temporal shape of the control fields for the MS gate typically require disentanglement conditions for all modes and a target accumulated geometric phase. To realize the protocol in Sec. IV, we instead aim for a nonzero displacement vector but have no requirement on the geometric phases that are accumulated in a single stage of the evolution, owing to driving a single spin at a time.

We assume that the control fields are decomposed into  $N_d$  intervals of duration  $\tau$ , maintaining a constant amplitude in each segment. Mathematically, they take the form  $\Omega_q^{(i)}(t) = \sum_{p=1}^{N_d} \Omega_{q,p}^{(i)} w(t/\tau, (p-1)\tau, p\tau)$  for  $q \in \{x, y\}$ , where  $w(t/\tau, (p-1)\tau, p\tau)$  is the rectangular window function returning 1 if  $(p-1)\tau \leq t < p\tau$  and zero otherwise.  $\Omega_{q,p}^{(i)}$  are the list of  $2N_d$  amplitudes that we aim to find and  $\tau_d = N_d\tau$  is the overall pulse duration. We use  $\tau_d = 50 \mu\text{s}$  and  $N_d = 40$ .

For driving a single spin, the target complex displacements correspond to Eq. (3), the matrix form of which is given by

$$\begin{pmatrix} \text{Re}(\alpha_{i1}) \\ \vdots \\ \text{Re}(\alpha_{iM}) \\ \text{Im}(\alpha_{i1}) \\ \vdots \\ \text{Im}(\alpha_{iM}) \end{pmatrix} = \begin{pmatrix} d_{11} & \cdots & d_{1M} & \tilde{d}_{11} & \cdots & \tilde{d}_{1M} \\ \vdots & \ddots & \vdots & \vdots & \ddots & \vdots \\ d_{M1} & \cdots & d_{MM} & \tilde{d}_{M1} & \cdots & \tilde{d}_{MM} \\ \tilde{d}_{11} & \cdots & \tilde{d}_{1M} & -d_{11} & \cdots & -d_{1M} \\ \vdots & \ddots & \vdots & \vdots & \ddots & \vdots \\ \tilde{d}_{M1} & \cdots & \tilde{d}_{MM} & -d_{M1} & \cdots & -d_{MM} \end{pmatrix} \times \begin{pmatrix} \Omega_{x,1}^{(i)} \\ \vdots \\ \Omega_{x,N_d}^{(i)} \\ \Omega_{y,1}^{(i)} \\ \vdots \\ \Omega_{y,N_d}^{(i)} \end{pmatrix}. \quad (\text{C1})$$

Here, we use the  $2M \times 2N_d$  matrix  $\mathbf{d}$ , the elements of which are given by

$$d_{kp} = -\eta_{nk} \text{sinc}\left(\frac{\delta_k \tau}{2}\right) \cos\left((p + \frac{1}{2})\delta_k \tau\right), \quad (\text{C2})$$

$$\tilde{d}_{kp} = +\eta_{nk} \text{sinc}\left(\frac{\delta_k \tau}{2}\right) \sin\left((p + \frac{1}{2})\delta_k \tau\right), \quad (\text{C3})$$

for  $1 \leq j \leq M$  and  $1 \leq p \leq N_d$ .

For the case  $N_D > M$  considered here, Eq. (C1) has an infinite number of solutions, meaning that there are many phase-space trajectories that can end at the target displacements vector at time  $\tau_d$ . Here, we calculate a single solution by applying the Moore-Penrose pseudoinversion in Eq. (C1). This particular operation yields the control field vector with the least norm among all solutions, corresponding to the wave form with the lowest average power.

### 2. Optimal control of spin-dependent scaling and rotations

To find the control fields  $\Omega_x^{(i)}(t), \Omega_y^{(i)}(t)$  that yield the target mode-mixing parameters  $\psi_{km}(\tau_s), \chi_{km}(\tau_s)$ , we use the open-source quantum optimal-control algorithm GRAPE, implemented in PYTHON [57,58]. We first simplify Eqs. (10) and (11) by describing the evolution in a frame that rotates at frequency  $\Delta_k/2$  by defining the rotated mixing parameters  $\tilde{\psi}_{km} = e^{i\Delta_k t/2} \psi_{km}$  and  $\tilde{\chi}_{km}^* = e^{-i\Delta_k t/2} \chi_{km}^*$ . Under these transformations, Eqs. (10) and (11) become

$$\partial_t \tilde{\psi}_{km} = \frac{i}{2} \Delta_k \tilde{\psi}_{km} - i \sum_l h_{kl} \tilde{\chi}_{lm}^*, \quad (\text{C4})$$

$$\partial_t \tilde{\chi}_{km}^* = -\frac{i}{2} \Delta_k \tilde{\chi}_{km}^* + i \sum_l h_{kl}^* \tilde{\psi}_{lm}, \quad (\text{C5})$$

where the time dependence is then determined only by the control fields in  $h_{kl}(t)$  [cf. Eq. (9)]. For the numerical implementation, we use a compact vector format

$$\bar{\psi}_m = (\tilde{\psi}_{1m}, \dots, \tilde{\psi}_{Mm}, \tilde{\chi}_{1m}^*, \dots, \tilde{\chi}_{Mm}^*)^T \quad (\text{C6})$$

and explicitly account for the spin state of the driven ions using the extended basis  $\psi_m = \tilde{\psi}_m \otimes |\sigma_n\rangle$ . Here,  $|\sigma_n\rangle$  are the computational-basis vectors of the spins in the  $x$  basis (i.e., corresponding to the eigenstates of the  $\sigma_x^{(i)}$  operators with eigenvalues  $\pm 1$  for all  $1 \leq i \leq N_S$ ), which enable the representation of all  $1 \leq n \leq 2^{N_S}$  spin configurations in Hilbert space. For practical implementation, we consider only the spin states that are associated with the  $N_S \leq N$  ions that are driven by the squeezing beams. While the Hilbert space grows exponentially with  $N_S$ , importantly, we note that  $N_S$  scales with the order of the interaction  $N$  and not with the number of ion spins in the chain  $M$ . For the applications we consider in this work, the exponential increase is modest because  $N_S = N - 2 = 2$  for the four body gate in Sec. VA and  $N_S = N = 4$  for the polynomial spin operator in Sec. VB.

To render the time-dependent transformation in Eqs. (C4) and (C5) compatible with the formalism of GRAPE, we

cast them in the form

$$\partial_t \psi_m = \mathcal{H} \psi_m, \quad (\text{C7})$$

where the symmetric matrix  $\mathcal{H}$  is given by

$$\mathcal{H} = \frac{i}{2} s_z \otimes \mathbf{\Delta} \otimes \mathbb{1}_\sigma + \frac{1}{2} \sum_{i=1}^M (\Omega_x^{(i)} s_x + \Omega_y^{(i)} s_y) \otimes \eta_i^2 \otimes \sigma_x^{(i)}. \quad (\text{C8})$$

We use  $\eta_i^2$  to denote the  $M \times M$  matrix the elements  $(\eta_i^2)_{mk} = \eta_{im} \eta_{ik}$  of which describe the coupling between the  $m$ th and  $k$ th modes via the  $i$ th ion.  $\mathbf{\Delta}$  denotes a diagonal  $M \times M$  matrix with nonzero elements  $\Delta_k$  on the diagonal. We denote by  $s_x, s_y,$  and  $s_z$  the  $2 \times 2$  Pauli matrices, which are unrelated to the spin operators but, rather, construct the correct relations between the mode-mixing parameters  $\tilde{\psi}_{mk}$  and  $\tilde{\chi}_{mk}^*$  in Eq. (C6). For clarity, we denote the identity spin matrix by  $\mathbb{1}_\sigma$ .

In this form, the operator  $\mathcal{H}$  is a  $(2^{N_S+1}M) \times (2^{N_S+1}M)$  matrix that can be decomposed into the time-independent drift Hamiltonian  $H_{\text{drift}} = \frac{i}{2} s_z \otimes \mathbf{\Delta} \otimes \mathbb{1}_\sigma$  and the  $2N_S$  control Hamiltonians taken from the set  $\{s_x \otimes \eta_{\mathbf{i}_n}^2 \otimes \sigma_x^{(\mathbf{i}_n)}, s_y \otimes \eta_{\mathbf{i}_n}^2 \otimes \sigma_x^{(\mathbf{i}_n)}\}$  with  $1 \leq n \leq 2N_S$ , where the vector  $\mathbf{i}_n$  denotes the indices of the interacting ions. We simultaneously solve these equations by considering an optimization toward an objective ‘‘gate’’  $X(\tau_s)$  the columns of which are composed of the target vectors  $\psi_m$ . As the dimensions of  $X$  are  $2^{N_S+1}M \times 2^{N_S}M$ , we technically expand it into a rectangular matrix by adding the  $2^{N_S}M$  column vectors  $(\tilde{\chi}_{1m}, \dots, \tilde{\chi}_{Mm}, \tilde{\psi}_{1m}^*, \dots, \tilde{\psi}_{Mm}^*)^T \otimes |\sigma_q\rangle$  for  $1 \leq q \leq 2^{N_S}$  and  $1 \leq m \leq M$  (which physically corresponds to the transformation of  $\hat{a}^\dagger$ ). We also assume that  $X(0)$  is the identity matrix. As the dynamics are not unitary but, rather, *complex* symplectic, we use the ‘‘GEN\_MAT’’ dynamic evolution type of the algorithm, the ‘‘trace difference’’ as the fidelity measure, and the BFGS algorithm for the optimization method. For the calculation in this work, we assume that the control fields are composed of up to 70 segments.

### 3. Performance estimation of the pulse shaping

We estimate the performance of the numerically calculated pulses using two different complementary metrics. The first metric estimates the overlap of the numerically calculated evolution operator  $S_1$  of a single squeezing stage with respect to the target evolution operator  $S_2$ . The error for an imperfect overlap depends on the projected quantum state; for simplicity, we consider the motional ground state and take the average error over all  $2^{N_S}$  spin configurations in the  $x$  basis. This first fidelity metric is given by

$$\mathcal{F}_1 = \frac{1}{2^{N_S}} \sum_{n=1}^{2^{N_S}} |\langle 0, \sigma_n | S_1 S_2^\dagger | 0, \sigma_n \rangle|^2. \quad (\text{C9})$$

To calculate this fidelity yet avoid an explicit representation of the motional operators using Fock states, we follow Ref. [89] and for each spin configuration labeled by  $1 \leq n \leq 2^{N_S}$  directly compute

$$\mathcal{F}_1 = \frac{1}{2^{N_S}} \sum_{n=1}^{2^{N_S}} \exp\left(\text{Tr}(\log(Q_3^{(n)}))\right), \quad (\text{C10})$$

where the operators

$$Q_3^{(n)} = \sqrt{\mathbb{1} - T_3^{(n)} T_3^{(n)\dagger}}, \quad (\text{C11})$$

$$T_3^{(n)} = (Q_1^{(n)})^{-1} (T_1^{(n)} + T_2^{(n)}) (\mathbb{1} + T_1^{(n)\dagger} T_2^{(n)})^{-1} Q_1^{(n)T} \quad (\text{C12})$$

are cast through the representation of the numerical ( $q = 1$ ) and target ( $q = 2$ ) transformation matrices  $r_q$  [cf. Eq. (A8)] by  $T_q^{(n)} = \tanh(r_q^{(n)})$  and  $Q_q^{(n)} = \text{sech}(r_q^{(n)})$ . The matrices  $r_q$  for  $q \in \{1, 2\}$  are block-diagonal matrices with  $1 \leq n \leq 2^{N_S}$  blocks, where  $r_q^{(n)}$  denotes the  $n$ th block. Similar to Appendix A, all of the above operations are full matrix operations.

The fidelity  $\mathcal{F}_1$  is sensitive predominantly to residual coupling of spin and motion with respect to the target evolution. To ensure that the overall target spin Hamiltonian is obtained, we calculate a second fidelity metric,

$$\mathcal{F}_2 = 1 - \frac{1}{2^N} \sum_{n_1, n_2} |\Phi_{n_1, n_2}^{(1)} - \Phi_{n_1, n_2}^{(2)}|, \quad (\text{C13})$$

where  $1 \leq n_1, n_2 \leq 2^N$ . The numerically calculated and target geometric phase operators,  $\Phi^{(1)}$  and  $\Phi^{(2)}$ , respectively, are numerically evaluated using Eq. (14). We recall that these geometric phases are associated with the effective spin Hamiltonians in Eq. (15) and are numerically represented in the  $x$  basis. Our numerical pulse-shaping optimization is stopped when the conditions  $(\mathcal{F}_1)^4, \mathcal{F}_2 > 0.999$  are both satisfied.

## APPENDIX D: EQUIVALENT QUANTUM CIRCUITS

The quantum circuits discussed in Sec. V C are shown in Fig. 8. The circuit in Fig. 8(a) constructs the stabilizer gate operator  $U = \exp(-i\Phi \sigma_z^{(0)} \sigma_z^{(1)} \sigma_z^{(2)} \sigma_z^{(3)})$  for qubits 0, 1, 2, and 3 presented in the  $z$  basis (in the main text we use the  $x$  axis; however, basis transformation can be realized with a set of one-qubit operations). It is decomposed of six CNOT gates (light-blue symbols) and a single one-qubit gate (light-red rectangles). The one-qubit operation acting on qubit  $i$  is given by either

$$U_3(\alpha, \beta, \gamma) = R_z^{(i)}(\beta) R_x^{(i)}(-\frac{\pi}{2}) R_z^{(i)}(\alpha) R_x^{(i)}(\frac{\pi}{2}) R_z^{(i)}(\gamma)$$

or by  $U_1(\alpha) = e^{i\alpha/2} R_z^{(i)}(\alpha)$ , where  $R_z^{(i)}(\alpha) = e^{-i\alpha \sigma_z^{(i)}/2}$  and  $R_x^{(i)}(\alpha) = e^{-i\alpha \sigma_x^{(i)}/2}$  are the operators rotating the qubit

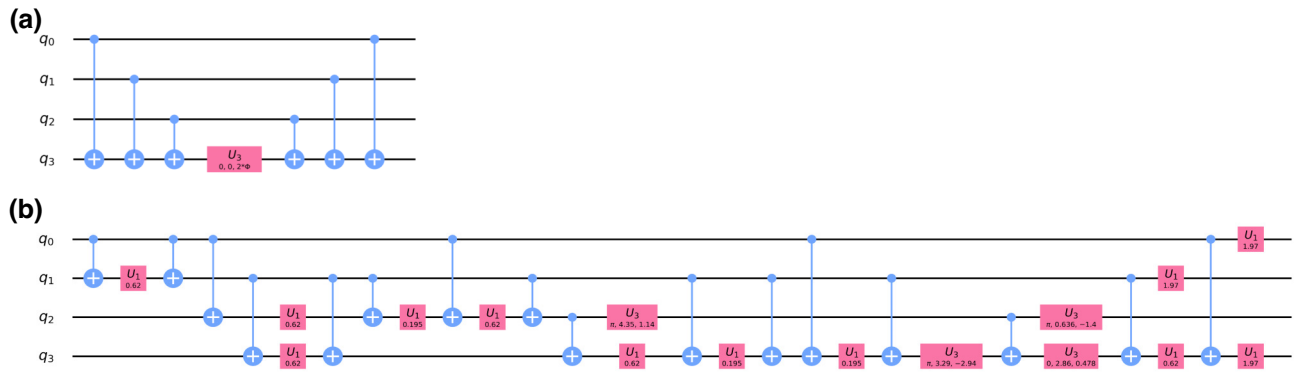


FIG. 8. Equivalent circuits for the gates in Secs. V A and V B in the main text that consist of (a) six and (b) 16 two-qubit gates, respectively.

around axes  $z$  and  $x$  in the Bloch sphere, respectively. The CNOT gates between qubits  $i$  and  $j$  are given by the operator  $\exp\left(-i\frac{\pi}{4}(\mathbb{1}_\sigma^{(i)}\mathbb{1}_\sigma^{(j)} - \sigma_z^{(i)}\mathbb{1}_\sigma^{(j)})(\mathbb{1}_\sigma^{(i)}\mathbb{1}_\sigma^{(j)} - \mathbb{1}_\sigma^{(i)}\sigma_x^{(j)})\right)$  and are equivalent to MS gates up to additional one-qubit gates.

The circuit in Fig. 8(b) composes the polynomial gate operator

$$U = \exp\left(-i\Phi \prod_{i=0}^3 (\mathbb{1}_\sigma^{(i)} + \tanh(\xi)\sigma_z^{(i)})\right),$$

for  $\xi = 0.325$  and  $\Phi = \pi$ . For this gate, we use numeric rather than parametrized values because this improves the transpiled circuit by the QISKIT optimizer in terms of the two-qubit gate count.

[1] C. Monroe, W. C. Campbell, L.-M. Duan, Z.-X. Gong, A. V. Gorshkov, P. W. Hess, R. Islam, K. Kim, N. M. Linke, G. Pagano, P. Richerme, C. Senko, and N. Y. Yao, Programmable quantum simulations of spin systems with trapped ions, *Rev. Mod. Phys.* **93**, 025001 (2021).  
 [2] T. Lubinski, S. Johri, P. Varosy, J. Coleman, L. Zhao, J. Necaie, C. H. Baldwin, K. Mayer, and T. Proctor, Application-Oriented Performance Benchmarks for Quantum Computing (2021), [ArXiv:2110.03137](https://arxiv.org/abs/2110.03137).  
 [3] J. I. Cirac and P. Zoller, Quantum Computations with Cold Trapped Ions, *Phys. Rev. Lett.* **74**, 4091 (1995).  
 [4] F. Mintert and C. Wunderlich, Ion-Trap Quantum Logic Using Long-Wavelength Radiation, *Phys. Rev. Lett.* **87**, 257904 (2001).  
 [5] A. Sørensen and K. Mølmer, Entanglement and quantum computation with ions in thermal motion, *Phys. Rev. A* **62**, 022311 (2000).  
 [6] G. Milburn, S. Schneider, and D. James, Ion trap quantum computing with warm ions, *Fortschr. Phys.* **48**, 801 (2000).  
 [7] E. Solano, R. L. de Matos Filho, and N. Zagury, Deterministic Bell states and measurement of the motional state of two trapped ions, *Phys. Rev. A* **59**, R2539 (1999).

[8] D. Porras and J. I. Cirac, Effective Quantum Spin Systems with Trapped Ions, *Phys. Rev. Lett.* **92**, 207901 (2004).  
 [9] Y. Shapira, R. Shaniv, T. Manovitz, N. Akerman, and R. Ozeri, Robust Entanglement Gates for Trapped-Ion Qubits, *Phys. Rev. Lett.* **121**, 180502 (2018).  
 [10] P. H. Leung, K. A. Landsman, C. Figgatt, N. M. Linke, C. Monroe, and K. R. Brown, Robust 2-Qubit Gates in a Linear Ion Crystal Using a Frequency-Modulated Driving Force, *Phys. Rev. Lett.* **120**, 020501 (2018).  
 [11] A. E. Webb, S. C. Webster, S. Collingbourne, D. Breaud, A. M. Lawrence, S. Weidt, F. Mintert, and W. K. Hensinger, Resilient Entangling Gates for Trapped Ions, *Phys. Rev. Lett.* **121**, 180501 (2018).  
 [12] M. K. Joshi, F. Kranzl, A. Schuckert, I. Lovas, C. Maier, R. Blatt, M. Knap, and C. F. Roos, Observing emergent hydrodynamics in a long-range quantum magnet, *Science* **376**, 720 (2022).  
 [13] L. Feng, O. Katz, C. Haack, M. Maghrebi, A. V. Gorshkov, Z. Gong, M. Cetina, and C. Monroe, (2022), [arXiv preprint ArXiv:2211.01275](https://arxiv.org/abs/2211.01275).  
 [14] Y. Shapira, T. Manovitz, N. Akerman, A. Stern, and R. Ozeri, Quantum Simulations of Interacting Systems with Broken Time-Reversal Symmetry, *Phys. Rev. X* **13**, 021021 (2023).  
 [15] J. T. Seeley, M. J. Richard, and P. J. Love, The Bravyi-Kitaev transformation for quantum computation of electronic structure, *J. Chem. Phys.* **137**, 224109 (2012).  
 [16] P. J. J. O'Malley, *et al.*, Einstein-Podolsky-Rosen Experiment with Two Bose-Einstein Condensates, *Phys. Rev. X* **6**, 031007 (2016).  
 [17] Y. Nam, J.-S. Chen, N. C. Pienti, K. Wright, C. Delaney, D. Maslov, K. R. Brown, S. Allen, J. M. Amini, J. Apisdorf, *et al.*, IBM Q Experience as a versatile experimental testbed for simulating open quantum systems, *npj Quantum Information* **6**, 1 (2020).  
 [18] A. Aspuru-Guzik, A. D. Dutoi, P. J. Love, and M. Head-Gordon, Simulated quantum computation of molecular energies, *Science* **309**, 1704 (2005).  
 [19] C. Hempel, C. Maier, J. Romero, J. McClean, T. Monz, H. Shen, P. Jurcevic, B. P. Lanyon, P. Love, R. Babush, *et al.*, Quantum Chemistry Calculations on a Trapped-Ion Quantum Simulator, *Phys. Rev. X* **8**, 031022 (2018).

- [20] M. C. Banuls, R. Blatt, J. Catani, A. Celi, J. I. Cirac, M. Dalmonte, L. Fallani, K. Jansen, M. Lewenstein, S. Montangero, *et al.*, Simulating lattice gauge theories within quantum technologies, *Eur. Phys. J. D* **74**, 1 (2020).
- [21] A. Ciavarella, N. Klco, and M. J. Savage, Trailhead for quantum simulation of SU(3) Yang-Mills lattice gauge theory in the local multiplet basis, *Phys. Rev. D* **103**, 094501 (2021).
- [22] P. Hauke, D. Marcos, M. Dalmonte, and P. Zoller, Quantum Simulation of a Lattice Schwinger Model in a Chain of Trapped Ions, *Phys. Rev. X* **3**, 041018 (2013).
- [23] R. C. Farrell, I. A. Chernyshev, S. J. M. Powell, N. A. Zemtsovskiy, M. Illa, and M. J. Savage, Preparations for quantum simulations of quantum chromodynamics in  $1 + 1$  dimensions. I. Axial gauge, *Phys. Rev. D* **107**, 054512 (2023).
- [24] A. Paetznick and B. W. Reichardt, Universal Fault-Tolerant Quantum Computation with Only Transversal Gates and Error Correction, *Phys. Rev. Lett.* **111**, 090505 (2013).
- [25] A. Y. Kitaev, Fault-tolerant quantum computation by anyons, *Ann. Phys. (NY)* **303**, 2 (2003).
- [26] J. K. Pachos and M. B. Plenio, Three-Spin Interactions in Optical Lattices and Criticality in Cluster Hamiltonians, *Phys. Rev. Lett.* **93**, 056402 (2004).
- [27] M. Müller, K. Hammerer, Y. Zhou, C. F. Roos, and P. Zoller, Simulating open quantum systems: From many-body interactions to stabilizer pumping, *New J. Phys.* **13**, 085007 (2011).
- [28] O. I. Motrunich, Variational study of triangular lattice spin-1/2 model with ring exchanges and spin liquid state in  $\kappa$ -(ET)  $2\text{Cu}2(\text{CN})3$ , *Phys. Rev. B* **72**, 045105 (2005).
- [29] B. Andrade, Z. Davoudi, T. Graß, M. Hafezi, G. Pagano, and A. Seif, Engineering an effective three-spin Hamiltonian in trapped-ion systems for applications in quantum simulation, *Quantum Sci. Technol.* **7**, 034001 (2022).
- [30] A. Bermudez, D. Porras, and M. Martin-Delgado, Competing many-body interactions in systems of trapped ions, *Phys. Rev. A* **79**, 060303 (2009).
- [31] V. Vedral, A. Barenco, and A. Ekert, Quantum networks for elementary arithmetic operations, *Phys. Rev. A* **54**, 147 (1996).
- [32] L. K. Grover, in Proceedings of the Twenty-Eighth Annual ACM Symposium on Theory of Computing (1996), p. 212.
- [33] X. Wang, A. Sørensen, and K. Mølmer, Multibit Gates for Quantum Computing, *Phys. Rev. Lett.* **86**, 3907 (2001).
- [34] T. Monz, K. Kim, W. Hänsel, M. Riebe, A. S. Villar, P. Schindler, M. Chwalla, M. Hennrich, and R. Blatt, Realization of the Quantum Toffoli Gate with Trapped Ions, *Phys. Rev. Lett.* **102**, 040501 (2009).
- [35] J. D. Arias Espinoza, K. Groenland, M. Mazzanti, K. Schoutens, and R. Gerritsma, High-fidelity method for a single-step  $N$ -bit Toffoli gate in trapped ions, *Phys. Rev. A* **103**, 052437 (2021).
- [36] C. Figgatt, D. Maslov, K. A. Landsman, N. M. Linke, S. Debnath, and C. Monroe, Complete 3-Qubit Grover search on a programmable quantum computer, *Nat. Commun.* **8**, 1 (2017).
- [37] I. Marvian, Restrictions on realizable unitary operations imposed by symmetry and locality, *Nat. Phys.* **18**, 283 (2022).
- [38] S. Lloyd, Universal Quantum Simulators, *Science* **273**, 1073 (1996).
- [39] O. Katz, M. Cetina, and C. Monroe,  $N$ -Body Interactions between Trapped Ion Qubits via Spin-Dependent Squeezing, *Phys. Rev. Lett.* **129**, 063603 (2022).
- [40] A. Sørensen and K. Mølmer, Quantum Computation with Ions in Thermal Motion, *Phys. Rev. Lett.* **82**, 1971 (1999).
- [41] S. Debnath, N. M. Linke, C. Figgatt, K. A. Landsman, K. Wright, and C. Monroe, Demonstration of a small programmable quantum computer with atomic qubits, *Nature* **536**, 63 (2016).
- [42] D. Zhu, G. D. Kahanamoku-Meyer, L. Lewis, C. Noel, O. Katz, B. Harraz, Q. Wang, A. Risinger, L. Feng, D. Biswas, *et al.*, (2021), arXiv preprint [ArXiv:2112.05156](https://arxiv.org/abs/2112.05156).
- [43] R. Stricker, J. Carrasco, M. Ringbauer, L. Postler, M. Meth, C. Edmunds, P. Schindler, R. Blatt, P. Zoller, B. Kraus, *et al.*, (2022), arXiv preprint [ArXiv:2203.07395](https://arxiv.org/abs/2203.07395).
- [44] D. Schwerdt, Y. Shapira, T. Manovitz, and R. Ozeri, Comparing two-qubit and multiqubit gates within the toric code, *Phys. Rev. A* **105**, 022612 (2022).
- [45] K. Seetharam, D. Biswas, C. Noel, A. Risinger, D. Zhu, O. Katz, S. Chattopadhyay, M. Cetina, C. Monroe, E. Demler, *et al.*, (2021), arXiv preprint [ArXiv:2109.13298](https://arxiv.org/abs/2109.13298).
- [46] A. Erhard, H. Poulsen Nautrup, M. Meth, L. Postler, R. Stricker, M. Stadler, V. Negnevitsky, M. Ringbauer, P. Schindler, H. J. Briegel, *et al.*, Entangling logical qubits with lattice surgery, *Nature* **589**, 220 (2021).
- [47] D. Leibfried, R. Blatt, C. Monroe, and D. Wineland, Quantum dynamics of single trapped ions, *Rev. Mod. Phys.* **75**, 281 (2003).
- [48] R. Srinivas, S. Burd, H. Knaack, R. Sutherland, A. Kwiatkowski, S. Glancy, E. Knill, D. Wineland, D. Leibfried, A. C. Wilson, *et al.*, High-fidelity laser-free universal control of trapped ion qubits, *Nature* **597**, 209 (2021).
- [49] T. Harty, M. Sepiol, D. Allcock, C. Ballance, J. Tarlton, and D. Lucas, High-Fidelity Trapped-Ion Quantum Logic Using Near-Field Microwaves, *Phys. Rev. Lett.* **117**, 140501 (2016).
- [50] R. Srinivas, S. C. Burd, R. T. Sutherland, A. C. Wilson, D. J. Wineland, D. Leibfried, D. T. Allcock, and D. H. Slichter, Trapped-Ion Spin-Motion Coupling with Microwaves and a Near-Motional Oscillating Magnetic Field Gradient, *Phys. Rev. Lett.* **122**, 163201 (2019).
- [51] D. J. Wineland, C. Monroe, W. M. Itano, D. Leibfried, B. E. King, and D. M. Meekhof, Experimental issues in coherent quantum-state manipulation of trapped atomic ions, *J. Res. Natl. Inst. Stand. Technol.* **103**, 259 (1998).
- [52] K. Kim, C. Roos, L. Aolita, H. Häffner, V. Nebendahl, and R. Blatt, Geometric phase gate on an optical transition for ion trap quantum computation, *Phys. Rev. A* **77**, 050303 (2008).
- [53] M. Cetina, L. Egan, C. Noel, M. Goldman, D. Biswas, A. Risinger, D. Zhu, and C. Monroe, Control of Transverse Motion for Quantum Gates on Individually Addressed Atomic Qubits, *PRX Quantum* **3**, 010334 (2022).
- [54] G. Cariolaro and G. Pierobon, (2017), arXiv preprint [ArXiv:1704.02008](https://arxiv.org/abs/1704.02008).
- [55] B. C. Hall, *Lie Groups, Lie Algebras, and Representations: An Elementary Introduction*, Graduate Texts in Mathematics, Vol. 222 (Springer, New York, 2010) p. 351 S.

- [56] X. Wang and P. Zanardi, Simulation of many-body interactions by conditional geometric phases, *Phys. Rev. A* **65**, 032327 (2002).
- [57] J. R. Johansson, P. D. Nation, and F. Nori, QuTiP: An open-source PYTHON framework for the dynamics of open quantum systems, *Comput. Phys. Commun.* **183**, 1760 (2012).
- [58] A. J. G. Pitchford, Ph.D. thesis, Department of Mathematics, Aberystwyth University (2019).
- [59] B. E. King, *Quantum State Engineering and Information Processing with Trapped Ions* (University of Colorado at Boulder, Boulder, 1999).
- [60] N. Schuch and J. Siewert, Programmable Networks for Quantum Algorithms, *Phys. Rev. Lett.* **91**, 027902 (2003).
- [61] J. Welch, D. Greenbaum, S. Mostame, and A. Aspuru-Guzik, Efficient quantum circuits for diagonal unitaries without ancillas, *New J. Phys.* **16**, 033040 (2014).
- [62] M. A. Nielsen and I. L. Chuang, *Quantum Computation and Quantum Information* (Cambridge University Press, Cambridge, United Kingdom, 2000).
- [63] M. Treinish, *et al.*, QISKIT 0.39.4, <https://qiskit.org> (2022).
- [64] L. Egan, D. M. Debroy, C. Noel, A. Risinger, D. Zhu, D. Biswas, M. Newman, M. Li, K. R. Brown, M. Cetina, *et al.*, Fault-tolerant control of an error-corrected qubit, *Nature* **598**, 281 (2021).
- [65] Y. Wang, S. Crain, C. Fang, B. Zhang, S. Huang, Q. Liang, P. H. Leung, K. R. Brown, and J. Kim, High-Fidelity Two-Qubit Gates Using a Microelectromechanical-System-Based Beam Steering System for Individual Qubit Addressing, *Phys. Rev. Lett.* **125**, 150505 (2020).
- [66] R. Blümel, N. Grzesiak, N. Pienti, K. Wright, and Y. Nam, Emergence and control of complex behaviors in driven systems of interacting qubits with dissipation, *npj Quantum Inf.* **7**, 1 (2021).
- [67] R. Blümel, N. Grzesiak, N. H. Nguyen, A. M. Green, M. Li, A. Maksymov, N. M. Linke, and Y. Nam, Efficient Stabilized Two-Qubit Gates on a Trapped-Ion Quantum Computer, *Phys. Rev. Lett.* **126**, 220503 (2021).
- [68] S. S. Bullock and I. L. Markov, Asymptotically optimal circuits for arbitrary n-qubit diagonal computations, *Quantum Inf. Comput.* **4**, 27 (2004).
- [69] Q. Wu, Y. Shi, and J. Zhang, Continuous Raman sideband cooling beyond the Lamb-Dicke regime in a trapped ion chain, *Phys. Rev. Res.* **5**, 023022 (2023).
- [70] Y. Lu, S. Zhang, K. Zhang, W. Chen, Y. Shen, J. Zhang, J.-N. Zhang, and K. Kim, Global entangling gates on arbitrary ion qubits, *Nature* **572**, 363 (2019).
- [71] C. Figgatt, A. Ostrander, N. M. Linke, K. A. Landsman, D. Zhu, D. Maslov, and C. Monroe, Parallel entangling operations on a universal ion-trap quantum computer, *Nature* **572**, 368 (2019).
- [72] T. Manovitz, A. Rotem, R. Shaniv, I. Cohen, Y. Shapira, N. Akerman, A. Retzker, and R. Ozeri, Fast Dynamical Decoupling of the Mølmer-Sørensen Entangling Gate, *Phys. Rev. Lett.* **119**, 220505 (2017).
- [73] F. Martínez-García, L. Gerster, D. Vodola, P. Hrmo, T. Monz, P. Schindler, and M. Müller, Analytical and experimental study of center-line miscalibrations in Mølmer-Sørensen gates, *Phys. Rev. A* **105**, 032437 (2022).
- [74] J. Wei and E. Norman, Lie algebraic solution of linear differential equations, *J. Math. Phys.* **4**, 575 (1963).
- [75] Z. Jia, S. Huang, M. Kang, K. Sun, R. F. Spivey, J. Kim, and K. R. Brown, Angle-robust two-qubit gates in a linear ion crystal, *Phys. Rev. A* **107**, 032617 (2023).
- [76] W. Morong, K. S. Collins, A. De, E. Stavropoulos, T. You, and C. Monroe, Engineering Dynamically Decoupled Quantum Simulations with Trapped Ions, *PRX Quantum* **4**, 010334 (2023).
- [77] O. Katz, L. Feng, A. Risinger, C. Monroe, and M. Cetina, (2022), arXiv preprint [ArXiv:2209.05691](https://arxiv.org/abs/2209.05691).
- [78] F. M. Gabbetta, W. Li, F. Schmidt-Kaler, and I. Lesanovsky, Engineering NonBinary Rydberg Interactions via Phonons in an Optical Lattice, *Phys. Rev. Lett.* **124**, 043402 (2020).
- [79] F. M. Gabbetta, C. Zhang, M. Hennrich, I. Lesanovsky, and W. Li, Long-Range Multibody Interactions and Three-Body Antiblockade in a Trapped Rydberg Ion Chain, *Phys. Rev. Lett.* **125**, 133602 (2020).
- [80] B. de Neeve, T.-L. Nguyen, T. Behrle, and J. P. Home, Error correction of a logical grid state qubit by dissipative pumping, *Nat. Phys.* **18**, 296 (2022).
- [81] C. Flühmann, T. L. Nguyen, M. Marinelli, V. Negnevitsky, K. Mehta, and J. Home, Encoding a qubit in a trapped-ion mechanical oscillator, *Nature* **566**, 513 (2019).
- [82] W. Chen, J. Gan, J.-N. Zhang, D. Matuskevich, and K. Kim, Quantum computation and simulation with vibrational modes of trapped ions, *Chin. Phys. B* **30**, 060311 (2021).
- [83] H. Gan, G. Maslennikov, K.-W. Tseng, C. Nguyen, and D. Matuskevich, Hybrid Quantum Computing with Conditional Beam Splitter Gate in Trapped Ion System, *Phys. Rev. Lett.* **124**, 170502 (2020).
- [84] S. Burd, R. Srinivas, J. Bollinger, A. Wilson, D. Wineland, D. Leibfried, D. Slichter, and D. Allcock, Quantum amplification of mechanical oscillator motion, *Science* **364**, 1163 (2019).
- [85] O. Katz and C. Monroe, (2022), arXiv preprint [ArXiv:2207.13653](https://arxiv.org/abs/2207.13653).
- [86] W. Chen, Y. Lu, S. Zhang, K. Zhang, G. Huang, M. Qiao, X. Su, J. Zhang, J.-N. Zhang, L. Bianchi, *et al.*, Scalable and programmable phononic network with trapped ions, *Nat. Phys.* **19**, 877 (2023).
- [87] W. Ge, B. C. Sawyer, J. W. Britton, K. Jacobs, J. J. Bollinger, and M. Foss-Feig, Trapped Ion Quantum Information Processing with Squeezed Phonons, *Phys. Rev. Lett.* **122**, 030501 (2019).
- [88] G. Cariolaro and G. Pierobon, Bloch-Messiah reduction of Gaussian unitaries by Takagi factorization, *Phys. Rev. A* **94**, 062109 (2016).
- [89] X. Ma and W. Rhodes, Multimode squeeze operators and squeezed states, *Phys. Rev. A* **41**, 4625 (1990).
- [90] F. M. Fernández, On the time evolution operator for time-dependent quadratic Hamiltonians, *J. Math. Phys.* **30**, 1522 (1989).
- [91] F. M. Fernández, Time-evolution operator and Lie algebras, *Phys. Rev. A* **40**, 41 (1989).